ERNEST S. MULAYA (Orcid ID : 0000-0002-8629-0832)

DR THOMAS PHILLIPS (Orcid ID : 0000-0002-6783-9092)

Article type : Research Article

Structural Geometry and Evolution of the Rukwa Rift Basin, Tanzania: Implications for Helium Potential

Ernest Mulaya[1,2], Jon Gluyas[2], Ken McCaffrey[2], Thomas Phillips[2], Chris Ballentine[3]

[1]School of Mines and Geosciences, University of Dar es Salaam, P.O. Box 35052, Dar es Salaam, Tanzania.

[2]Department of Earth Sciences, Durham University, Durham, UK, DH1 3LE.

[3]Department of Earth Sciences, University of Oxford, Oxford, UK, OX1 3AN.

Ernest Mulaya (Corresponding author); Email: ernest.s.mulaya@durham.ac.uk

Abstract

The Rukwa Rift Basin, Tanzania is regarded as a modern example of cratonic rift zone despite complex polyphase extensional and episodic inversion structures. We interpret 2D seismic reflection data tied to wells to identify and describe structures controlling stratigraphic sequences (Late Carboniferous to Pleistocene) in two main segmented Rukwa Rift domains, A and B, which are controlled by the Chisi and Saza shear zones. Fault geometry and stratal patterns are illustrated in relation to their kinematic interaction with folds. Fold structures reflect both extensional and compressional deformation and were mapped with a particular interest for their helium potential. We illustrate fault bend folds, fault propagation folds and fault propagation monoclines that

are related to extension events. Folds related to compression exhibit various structural styles reflecting at least two phases of episodic and widespread inversion. Firstly, Early Jurassic inversion phase which involved multi-faulted anticlines in the Karoo strata. Secondly, a mild and widespread inversion structures during the Pleistocene which are characterized by both symmetrical and asymmetrical anticlines styles. Taken together, the extensional and compressional fold structures, stratal juxtapositions and unconformities define stratigraphic packages that are widely distributed in the Rukwa Rift Basin, and form potential subsurface traps for helium-nitrogen rich gases, from which some seep to the surface, evidently documented in thermal springs across the region.

Keywords: Rukwa Rift Basin; rift border faults; inversion styles; fault rotated fold styles; thermal springs; helium-nitrogen gases

1.0 Introduction

The Rukwa Rift Basin (RRB) is located within the western arm of the East African Rift System (EARS) near an intersection of the Victoria-Nubia-Rovuma-San tectonic plates (Chorowicz, 2005; Saria et al., 2014; Stamps et al., 2018; Wedmore et al., 2021; Fig. 1A-B). This basin has an axial length of ca. 300 km, widening from 40 to 80 km progressively towards the southeast (Fig. 1B). The RRB records multiple stages of tectonic rifting from the Palaezoic, Mesozoic and Cenozoic (Ebinger, 1989; Morley, 1989; Sander & Rosendahl, 1989; Roberts et al., 2012; Fig. 2). Previous authors have suggested that this rift basin is a reactivated system of Neoproterozoic sinistral shear zones within the NW-trending Palaeoproterozoic Ubende belt on the western margin of the Archean-Tanzanian Craton (e.g. Quennell et al., 1956; Wescott et al., 1991; Lenoir et al., 1994; Delvaux et al., 1992; Morley et al., 1992; Theunissen et al., 1996). These earlier studies based on limited datasets inferred a number of tectonic extension directions for the Rukwa Rift which fall into three end-member models - NW-SE, NE-SW and E-W directions (e.g. Chorowicz and

Mukonki, 1980; Ebinger, 1989; Sander and Rosendahl 1989; Morley et al., 1992; Mbede, 1993; Wheeler and Rosendahl, 1994; Delvaux et al., 2012). However, the recent published geodetic data observation, Kostrov summation analyses of local teleseismic earthquakes data and source mechanisms for stress inversion, indicate present-day E-W extension rates ca. 2.26 mm y^{-1} (Delvaux and Barth, 2010; Saria et al., 2014; Stamps et al., 2018; Lavayssière et al., 2019). First-motion focal mechanism solutions for earthquakes reveal deformation from normal dip slip to strike slip on steep nodal planes (≥45°) with modal depths of 25–35 km (e.g. Delvaux et al., 2010; Lavayssière et al., 2019). Yet critical questions remain regarding the spatial and temporal distribution and evolution of structures, their kinematics interpretations and which have profound implications for helium potential at kilometer-scale depths within unconformably-bound synrift sedimentary packages.

Geochemical studies of surficial seepages of thermal springs and soils in the RRB have recently confirmed that they contain up to 10% helium by volume, with nitrogen dominating as a carrier gas (James, 1967a; James, 1967b; Barry et al., 2013; Danabalan, 2017). It is worth noting that such high concentrations of helium are exceptional in nature and substantially above the commonly accepted concentration of 0.3% for economically viable extraction of helium (Danabalan, 2017). Unlike the conventional helium occurrences associated with hydrocarbon in many places, the RRB presents a 'pure play' prospect where radiogenic helium is associated with nitrogen and carbon dioxide gases (e.g. Danabalan, 2017). The radiogenic helium, transported into the overlying sediments of the RRB, is inferred to originate from the surrounding Archean-aged Tanzania Craton or underlying Proterozoic basement (e.g. Holland et al., 2013; Warr et al., 2018). The release of the deep helium from its source is hypothesised to have been enhanced by recent tectonic and volcanic activity associated with the Cenozoic East African Rift System (Barry et al., 2013; Danabalan, 2017). All these factors make the RRB an ideal

location to examine how the structural heterogeneities formed during the evolution of the RRB contribute to its helium potential.

This study integrates well-tied 2D seismic reflection data, field observations and satellite imagery interpretations to address the question of how the rift geometry and structural styles have influenced basin stratigraphic distribution and helium potential for the RRB.

2.0 Regional Geologic and Tectonic Setting

2.1 Geology, tectonic terranes and shear zones

The RRB lies within the NW-trending Paleoproterozoic Ubendian orogenic belt at the southwestern margin of Tanzania between the Tanzanian Craton and the Archean-Paleoproterozoic Bangweulu Block (Kilembe and Rosendahl, 1992). The basin is surrounded by uplifted Paleoproterozoic basement that comprises mainly granulite and amphibolite facies metamorphic rocks with granitic intrusions (Daly, 1988; Kilembe and Rosendahl, 1992; Delvaux et al., 2012; Fritz et al., 2013). These basement units are subdivided into eight terranes, which are separated by ductile shear zones. These terranes include; Katuma, Lupa, Upangwa, Mbozi, Kate-Kipili, Ufipa, Wakole and Ubende Terranes (Boniface et al., 2012; Fig. 3A). These Precambrian terranes surrounding the RRB reveals three dominant lineament orientations of NW-SE, NNW-SSE and NNE-SSW (Fig. 3A).

The major shear zones in the Ubendian orogenic belt include; the Mughese shear zone, the Mutose shear zones, the Chisi shear zone and the Saza shear zone (Mnali, 1999; Boniface et al., 2012; Fig. 3A). Notably the Chisi shear zone, which defines a suture, marks the edge of the Ubendian orogenic belt and separates the Archaean to Palaeoproterozoic Bangweulu cratonic block from the Archean Tanzania Craton (Boniface et al., 2012; Delvaux et al., 2012; Heilman et al., 2019). These tectonic terranes

and shear zones significantly influence the geometry and syn-rift sediment distribution within the RRB, which we discuss in this study.

2.2 East Africa Rift System

The current tectonic setting of the N-S trending East African Rift System (EARS) extends from the Afar depression in Ethiopia through eastern Africa, stretching to the Southwest Indian Ridge i.e. at the junction with the Antarctic plate (e.g. Saria et al., 2014; Stamps et al., 2018; Fig. 1A). The EARS forms a divergent plate boundary mainly between the Nubian and the Somalian tectonic plates from which strains are accommodated along the Victoria, Rovuma, San and Lwandle subplates (Fernandez et al., 2004; Saria et al., 2014; Stamps et al., 2018; Daly et al., 2020; Wedmore et al., 2021). The EARS initiation dates back to the early Miocene and exhibit various active faulted-basins, frequent seismicity and volcanic centers (Ebinger, 2005; Saria et al., 2014). The EARS bifurcates into the Eastern and Western rift branches influenced by several zones of inherited basement fabrics (Daly et al., 1989; Theunissen et al., 1996; Chorowicz, 2005; Fig.1A). The Western branch exhibits several rifts occupied by large, mainly deep lakes from north to south including Lakes Albert, Edward, Kivu, Tanganyika, Rukwa and Nyasa (Malawi) and it continues to the Indian Ocean (Saria et al., 2014; Katumwehe et al., 2015; Lemna et al., 2019). The Rukwa Rift is located between the Victoria and Nubia plate near the intersection of the Victoria-Nubia-Rovuma- San plates (Fig. 1B).

2.3 Generalized stratigraphy of the Rukwa Rift Basin (RRB)

The stratigraphic sequences in the RRB include three major sedimentary packages overlying Precambrian basement namely: the Karoo Supergroup, the Red Sandstone Group and the Lake Beds Group (Quennell et al., 1956; Wescott et al., 1991; Morley et al., 1992; Mtelela, 2016; Fig. 2). The Karoo Supergroup comprises the Late Carboniferous to Permian units that lie unconformably on Precambrian Basement (Kilembe and

Rosendahl, 1992; Morley et al., 1999b; Fig. 2). The Red Sandstone Group unconformably overlies the Karoo Supergroup and is divided into two formations including the Cretaceous fluviatile Galula Formation, and the Oligocene Nsungwe Formation composed of mainly quartzose and richly fossiliferous fluvial-lacustrine sandstone sequences (Roberts et al., 2010; Mtelela et al., 2017; Widlansky et al., 2018). Finally, the uppermost strata consist of Late Miocene-Pleistocene Lake Beds Group which comprises two subdivisions including the Late Miocene-Pliocene Malangali Formation and the Pleistocene Ilasilo Formation (Hilbert-Wolf et al., 2017; Mtelela et al., 2017; Fig. 2). The uppermost strata contain records of the modern tectonic development of the EARS and associated extensive influence from the Rungwe Volcanic Provinces (RVP) (Ebinger et al., 1989; Wescott et al., 1991; Mtelela, 2016; Lawrence et al., 2021).

3.0 Methods and datasets

In this study the results from borehole-constrained 2D seismic reflection data, Digital Elevation Model (DEM) data and fieldwork are integrated to document structural and stratigraphic evolution of the RRB. This combined approach provides insights into the geometric and physiographic distribution of faults, stratigraphic units and their spatial relationships to rift-related structures (e.g. Hayward and Graham, 1989; Morley et al., 1999b; Turner and Williams, 2004; Phillips et al., 2020; Gluyas and Swarbrick 2021).

3.1 Datasets

3.1.1 Digital Elevation Models (TANDEM X-90m data)

We compiled TanDEM-90m (TerraSAR-X add-on for Digital Elevation Measurements) data, which were acquired by the German Aerospace Center (DLR) in partnership with Airbus Defence and Space between 2010 and 2015 (Rizzoli et al., 2017). These data are products of an Earth observation radar mission consisting of a Synthetic Aperture Radar (SAR) interferometer (Wessel, 2016). The acquisition involved the separation between

two identical satellites by 120 m to 500 m to create a 3D map of the Earth's land surfaces (Zink et al., 2014; Wessel, 2016). The TanDEM-X 90 m data provides a global Digital Elevation Model (DEM) with a 0.4 arcseconds (12 m) horizontal spatial resolution, and pixel spacing of 3 arcseconds corresponding to approximately 90 m at the equator, which is ideal for the purpose of this study (Zink et al., 2014; Wessel, 2016; Rizzoli et al., 2017).

3.1.2 Seismic and borehole data

The 2D seismic data used in this study were acquired by American Oil Company (AMOCO), Pecten, and Petrofina under a production sharing agreement with the Tanzania Petroleum Development Corporation (TPDC) in the 1980's while exploring for hydrocarbons in the area (Kilembe and Rosendahl, 1992; Morley et al., 1992). A land seismic program of 840 km was recorded with 64 - fold coverage using LRS 309 vibrators by Western Geophysical and 1610 km with 48 - fold acquired by Seiscom Delta in the Lake Rukwa (Morley et al., 1992), which occupies almost a half of the ca. 5800 km^2 depression formed adjacent to the Lupa Fault. The survey included a total of ca. 2450 km of 2D seismic lines spaced between 2.5-5.0 km apart stored in SEG-Y format. This operation resulted in the drilling of two dry wells namely Ivuna-1 and Galula-1, to depths of 7600 ft. (2317 m) penetrating the basement and 5000 ft. (1524 m) respectively (Wescott et al., 1991; Morley et al., 1992; Table 1). The two wells yielded wireline logs and formation tops data that are used to constrain the mapped seismic horizons (Fig. 2).

The seismic data are presented in Two Way Travel time (TWT). They are displayed with SEG reverse polarity, such that a downward increase in acoustic impedance is represented by a trough (blue) whereas a downward decrease in acoustic impedance is represented by a peak (red) reflection event on a seismic profile (Avseth et al., 2010). The seismic data are characterized by continuous and distinct medium to high energy events, however some places show low energy discontinuous and chaotic reflections with significantly degraded image quality. Thus, the datasets are in places of good quality and

optimal to ca. 6000 ms TWT depth to the Precambrian Basement, whereas in other areas the image quality is poor thus compromising the image resolution. The variability of the resolution across the dataset is reflected in some of the maps and seismic sections presented in this study.

3.2 Methods

3.2.1 Lineament mapping

Examination of the TanDEM-X 90 m derived hill shade and color-coded aspect maps enabled networks of topographic lineaments to be mapped. The lineaments were mapped to show the current spatial relationship between the traced structures and the distribution of thermal springs across the region which provides fundamental constraints on the fluid flow. Multiple directions of these lineaments are assumed to depict fault systems, fracture zones, mineral fabric orientations, and striking dyke structures or shear zones (e.g. Kervyn et al., 2006; Smets et al., 2016; Fig. 3). Using the shaded relief maps, topographic lineaments were identified and traced in ArcGIS software and calibrated by the existing field maps (e.g. Kervyn et al., 2006). The geometry of mapped lineaments was analysed using Stereonet™ software based on algorithms illustrated by Allmendinger et al. (2013). Nevertheless, there are a number of caveats which concern the validity of this methodology and misinterpretation cannot be totally excluded. Some minor faults might be missed entirely due to small displacement and limited resolution to map structures from synrift outcrops.

3.2.2 Seismic data interpretation

Both seismic and well data were uploaded to Schlumberger's Petrel Software™ version 2018. The seismic data interpreted on an interactive workstation provide snapshots and important constraints on the subsurface potential for helium resources the RRB. Before interpretation, quality control of the seismic sections and horizons was performed using synthetic seismograms and lithological logs to tie the stratigraphic data to the seismic

reflection data (Roe et al., 1996; Fig. 2). During interpretation the major stratigraphic top reflectors were identified on a well-constrained 2D seismic image and picked based on borehole data and checkshot surveys from the Ivuna-1 well (Fig. 2). Four major seismic sequences were identified and interpreted corresponding to the Precambrian basement, Karoo Supergroup, Red Sandstone Group and Lake Beds sequences. The major seismic reflectors confining the stratigraphic sequences were mapped across the data coverage and the approximate depths shown in TWT. Consequently, time-thickness maps derived from major strata were generated using a convergent interpolation algorithm embedded in Petrel software.

Table 1. Well tops and the lithological boundaries extracted from drilling and geological report with End of Hole (E.O.H)(Morley et al., 1992; Roe et al., 1996).

Well Name	Top Horizon	Depth (ft)
Ivuna-1 (E.O.H=7600 ft)	Top Nsungwe Formation	2233
	Top Upper Karoo Formation	4950
	Top Precambrian Basement	7540
Galula-1 (E.O.H=5000 ft)	Top Nsungwe Formation	5000

4.0 Results

4.1 Rift geometry, physiography and stratigraphy

Major fault networks in the RRB consist of two border faults, the NW-trending Lupa Fault to the east and the Ufipa Fault to the west which are broadly collinear with the general rift trend and extend up to c. 350 km and c. 400 km respectively (Fig. 3A-C; Fig. 4). The Lupa Fault terminates abruptly in the northwest and becomes buried in the Rungwe volcanic province in the southeast and thus it is no longer visible at the surface (Fig. 3A). To the west and southwest the RRB is bordered by the NW-trending Ufipa Fault, which abuts the Chisi shear zone in the northwest (Kervyn et al., 2006, Heilman et al., 2019; Fig. 3A; Fig. 4).

Intrabasinal faults are characterized by km-scale normal faults, which are either parallel to border faults or exhibit NNE-SSW and NNW-SSE orientations Fig. 3A-C; Fig. 4). The spatial and temporal variation of the border faults, shear zones and the intrabasinal fault networks exert control over synrift sedimentary packages and stratigraphic distribution in the RRB (e.g. Fig. 3A-C). Based on these structural patterns, we have divided the RRB into two structural domains; namely Domain A and Domain B (Fig. 4).

4.1.1 Domain A - Steep faults and gently-dipping synrift package wedge

Domain A extends northwestward from the northern end of the Mbozi Block (Fig. 4). In this domain, the Lupa Fault exhibits planar geometry at all mapped depths (Fig. 5A). Within 5 - 10 km of the Lupa Fault, the RRB is characterized by steeply NE-dipping antithetic normal faults whereas in the middle of basin it is dominated by steeply dipping conjugate faults between which strata are mildly folded (Fig. 5A). Further to the west of the RRB, steeply dipping normal faults, that are synthetic faults to the Ufipa Fault, dominate and are aligned with the Chisi shear zone (Fig. 3A; Fig. 4).

The RRB in Domain A is characterized by gently dipping synrift stratal wedges that show overall thickening to c. 3500 ms TWT towards the Lupa Fault in a region covering the entire basin north of the Mbozi Block (Fig. 5A). In this domain the Karoo Supergroup and the Red Sandstone Group exhibit a progressively thickening wedge morphology that dips gently towards the Lupa Fault whereas the Lake Beds strata are relatively shallowly dipping and display constant thickness of c. 1600 ms TWT. Generally the synrift strata range between 2500 and 3500 TWT ms, and are considerably thinner than the equivalent units in Domain B (Fig. 5A; Fig. 6).

4.1.2 Domain B - Rotated faults and steep synrift package wedge

In Domain B, the Lupa Fault dips more steeply than in Domain A in the upper section and more gently in the lower section (Fig. 6). In the middle of the basin c. 25 km from the

Lupa Fault, we map a major intrabasinal rotated fault with a general NW-strike and SW-dip extending through the entire Domain B (cf. Fig 4 to see map extent). This fault exhibits a curvilinear pattern in map-view and rotational geometry in cross section (Fig. 4; Fig. 6). Adjacent to the Mbozi Block, Domain B is characterized by predominantly NNW-SSE and NNE-SSW striking faults/lineaments, which extend into the Mbozi Block and the RRB (Fig. 3A).

The geometry of the RRB in Domain B is that of a classical half-graben in which the sedimentary packages thicken and dip towards the Lupa Fault (Fig. 6). The basin thickness varies from zero across the uplifted Mbozi block and the Ufipa Fault in the southwest thickening to 6000 ms TWT adjacent to the Lupa Fault. The synrift sedimentary packages in this domain are generally thicker than their coeval packages within Domain A (Fig. 5A; Fig. 6). Notably the Karoo Supergroup in this domain exhibits two distinctly different seismic characters and structural styles. The lower part of the Karoo sequences sequence is highly faulted, whilst the upper sequence remains relatively undeformed (Fig. 6). A high-amplitude seismic reflector, which separates the upper and lower sequences, exhibits distinct continuity across the basin (Fig. 6). Based on these seismic signatures observed in Domain B, we divide the Karoo Supergroup into two subdivisions, herein named the Upper Karoo Formation and Lower Karoo Formation. These distinct intervals most likely record the Karoo Supergroup deposition between late Carboniferous (Pennsylvanian) – Permian (Cisuralian) and late Permian (Lopingian) respectively with a hiatus that is possibly Guadalupian age (cf. Delvaux, 2001; Mtelela et al., 2017; Hilbert-Wolf et al., 2017; Widlansky et al., 2018; Fig. 2; Fig. 6).

4.1.3 Border fault segmentation and transfer zones

The Lupa and the Ufipa faults exhibit discrete ca. 25 km and 20 km length border fault segments respectively located approximately at 8° S which we name the Saza and Kwera transfer faults (Fig. 4). By transfer fault we refer to a dip-slip fault segment between two major border fault segments, which have slightly different displacement and geometry

components i.e. a transitional zone of deformational strain from fault to fault (e.g. Walsh and Watterson, 1989). These structures bound a region that we have named the Kwera - Saza Accommodation Zone (KSAZ) (Fig. 3A). The transfer fault segment separates the border faults into northern and southern segments and acts as a transition zone between Domain A and B (Fig. 3A; Fig. 4). These transfer segments are separated from the main border fault segments by a gap of up to ca. 3 - 5 km at both ends of the fault traces (Fig. 4). The surface trace of these fault segments are characterized by a deviation from the main NW-SE trend of border faults to the NNW-SSE and WNW-ESE along the Lupa and the Ufipa Fault respectively (Fig. 4). These segments are possibly associated with a relay ramp (cf. Gawthorpe et al., 1990; Gawthorpe and Hurst 1993).

The time-structural map reveals that, the KSAZ is characterized by sediment accumulation minima and ESE-trending normal faults (Fig. 4). Notably across the KSAZ we see a transition zone separating the contrasting stratigraphic packages in Domain A and B along the strike length (cf. section 4.1.1 and 4.1.2; Fig. 4). West of the RRB, the stratigraphy across the KSAZ is characterized by a topographic basement high associated with uplift, erosion surfaces and truncation of Karoo strata (Fig. 7A-B).

4.2 Fault control on thermal springs and helium seeps

Thermal springs which are associated with helium in the RRB are mainly controlled by border faults and intrabasin fault networks (e.g. Figs. 8A-C). The intrabasin faults traced particularly at the northern end of the Mbozi Block in the Itumbula and Ivuna areas consist of a series of isolated faulted blocks and rotated sedimentary wedges (Figs. 8A-B). The Karoo and the Red Sandstone sequences are juxtapositioned along NW-SE and NNW-SSE striking normal faults associated with throws up to 630 ms TWT (Fig. 8B). These strata show significant thickness increase between 430 and 710 ms TWT towards the SW - dipping normal faults set (Fig. 8B).

Field observations reveal numerous sites which exhibit thermal springs with significant helium concentration in the RRB (e.g. Fig. 8A; Table 2). These thermal springs are distributed adjacent to the northern end of the Mbozi Block and along the Lupa Fault (Fig. 8A). Notably, in the vicinity of the Itumbula and Ivuna areas, surface manifestations reveals that the thermal springs with gas are bubbling into the salt pan at the boundary between the Precambrian basement and the synrift sediments (e.g. Figs. 8B-C). The combined seismic cross sectional views and surface manifestation of thermal springs from the Ivuna and Itumbula sites reveal that these fluids emanate from both NW-SE and NNW-SSE striking faults and at the lithological contact between the sedimentary units and the Precambrian basement (e.g. Figs. 4 & 8B-C). The geochemical analysis of fluid samples from these two sites in particular, show low $^{3}He/^{4}He$ ratios and high radiogenic helium concentration between 2% and 5% v/v associated with high nitrogen gas up to 96% (Danabalan, 2017; Table 2). The abundance of radiogenic helium concentrations in this part of the RRB confirms that the source rock is crystalline basement which is rich in helium producing minerals, i.e. uranium and thorium.

Table 2. Sample sites showing nitrogen and radiogenic helium concentrations. The $^{3}He/^{4}He$ ratios from samples are normalised to the atmospheric $^{3}He/^{4}He$ ratio of 1.4×10^{-6} (designated as 1 Ra). These results were also extracted from Danabalan, (2017) (see figure 8A for sample sites locations).

Sample site	^{4}He concentration (cm^3 STP) (x 10^{-2})	N_2 concentration (cm^3 STP)	$^{3}He/^{4}He$ (Ra)	References
1. Ivuna	2.5	0.96	0.18	Barry et al. (2013)
2. Itumbula	4.2	0.96	-	James, (1967a)
3. Lupa	0.005	-	3.45	Barry et al. (2013)
4. Lupa	0.02	-	3.75	James, (1967a)
5. Lupa	0.001	-	1.21	James, (1967a)

6. Songwe	-	-	1.19	Barry et al. (2013)
7. Songwe	-	-	3.61	Barry et al. (2013)

4.3 Fold structures and styles

The RRB exhibits various fold styles, which are collocated with the normal faults and are widely distributed across Domain A and B. In Domain A, two sets of folds are identified associated with ca. 10% of the faults within the Lake Beds sequences (Fig. 5A); The first fold set consists of symmetrical fold structure mapped between high angle conjugate normal faults (Fig. 5B). The second set is characterized by asymmetrical folds of stratigraphy in the hanging wall of normal faults that are antithetic to the Lupa Fault (Fig. 5C).

In Domain B, the Red Sandstone and Lake Beds sequences are deformed by asymmetric folds in the immediate hanging wall of the Lupa Fault in the southeast part of the basin (Fig. 9A-B). These folds verge towards the hanging wall of the Lupa Fault with fold axis roughly striking WNW-ESE. The amplitudes of these folds progressively decrease upwards to zero from a maximum of 140 ms at a depth of 3000 ms TWT (Fig. 9B). The Lupa Fault shows a relatively steeply dipping upper segment and a gently dipping lower segment while the folded strata dip toward the fault (Fig. 9B). We interpret these structures as fault bend folds formed as a passive response to the hanging wall moving past the dip change inflection point on the Lupa fault at depth.

Proximal to the northern end of the Mbozi Block, the folds exhibit amplitudes ca. 60 ms TWT and wavelength c. 3.5 km and are associated with the upward termination of normal faults, i.e they exhibit upward transition from faulting to folding (Fig. 9C). Within these faults, the synrift strata show sagging in the hanging wall synformal structure, most likely due to differential compaction and loading, i.e variation of thickening and thinning affecting both the Oligocene Nsungwe Formation and the lower Lake Beds

sequences (Late Miocene-Pliocene Malangali Formation) (e.g. Mtelela et al., 2017; Hilbert-Wolf et al., 2017; Fig. 9C). The synkinematic wedges and onlaps indicate that these folds initiated in the Oligocene (c. 25-26 Ma) and deformation continued until the Pleistocene (c. 2.6 Ma?) (cf. Roberts et al., 2012; Hilbert-Wolf et al., 2017). We interpret these structures as fault propagation folds formed above the tip of propagating blind normal faults. The combination of progressive fault propagation, displacement, folding and sedimentation produce a rotation of the wedge-shaped sedimentary packages, which thicken towards the hanging wall of the intrabasin faults.

Furthermore, in the middle of the basin within Domain B, sedimentary units older than the Lake Beds sequences at depths below 1.0 s TWT are folded with alternating anticlines in the footwall and synclines in the hanging wall of a major SW-dipping fault (Fig. 9D). We infer that the SW-dipping fault created an upward widening zones of distributed monoclinal flexural deformation (trishear) which were later breached by the faults (Fig. 9D). In the Lake Beds sequences only the lower most units are rotated and constantly dip away from the master faults as a result of fault propagation (Fig. 9D). In contrast, the uppermost sequences of the Lake Beds exhibit locally uplifted strata relative to the adjacent block and show a compressional phase (Fig. 9D). We interpret these extensional structures as fault-propagation monoclines.

4.4 Inversion phases and styles

The diagnostic features and extent of inversion structures are mapped and described in the context of potential traps for a helium-rich gas phase. The description is based on genetic mechanisms and kinematic relationships between faults and fold systems (e.g. Withjack et al., 2002).

We mapped a Karoo-aged inversion phase characterized by open and low amplitude (up to c. 150 ms), anticlines involving several faults (cf. Fig. 8B). These structures are located

in the southwest of the basin adjacent to the Ufipa Fault and the northern end of the Mbozi Block (cf. Fig. 8A). The anticlines involving Karoo sequences are inverted and the SW limb onlaps onto the Mbozi Block (Fig. 8B). These inversion structures are mapped within the Karoo strata and are overlain by Cretaceous Red Sandstone sequences (Fig. 8B). The seismic data suggest that the inversion phase occurred after the deposition of the last Karoo sediment and just before the first sediment deposition of the Red Sandstone Group during the Cretaceous. Based on this evidence, we infer that, these multifaulted anticlines represent an inversion phase that was active during the Middle Mesozoic, possibly in the Early Jurassic.

The younger inversion structures in the RRB are recorded only in the Lake Beds sequences and occur in two styles (Fig. 10A). Firstly, asymmetrical anticlines, which have a relatively steeper forelimb, that verge towards the hanging wall of adjacent NE - dipping faults (Fig. 10A). These structures occur in the antithetic faults to the Lupa Fault (Fig. 10A). The fold axes are sub-parallel to the Lupa Fault striking NW - SE. They extend remarkably parallel to the Lupa border fault with amplitudes that ranges between 100 - 150 ms within Domain A (Fig. 4; Fig. 10A).

The second inversion style is characterized by anticlines that form symmetric boxfold geometries with low-amplitudes 80 - 120 ms TWT (Fig. 10A). These anticlines appear as fault - parallel symmetrical folds of synrift units between steeply dipping conjugate normal faults (Fig. 10A-B). They form away from the main Lupa Fault and are traceable along strike in both Domains A and B (Fig. 4). The synkinematic strata mapped in the uppermost part of the Lake Beds sequences reveal that these structures formed due to mild, but widespread inversion during the latest Pleistocene age (Fig. 10B).

5.0 Discussion

5.1 Rift geometry and structural patterns

Our results suggest that the RRB exhibits a gently dipping sedimentary wedge and typical half graben geometries in Domain A and B respectively, consisting of tectonically controlled synrift sedimentary units with maximum sediment thickness recorded for each sequence adjacent to the Lupa Fault (cf. Fig. 5A; Fig. 6). The half-graben geometry in Domain B is thus partly similar to results of Rosendahl et al. (1986) and Ebinger, (1989). The overall geometry suggest that both Karoo and post-Karoo extensional strains were partitioned between Domain A and B (Figs. 3A & 4). In Domain A the extensional strains were accommodated by the Lupa Fault and the Chisi shear zone which most likely accommodated the formation of parallel synthetic normal faults to the Ufipa Fault (Figs. 3A & 4). In Domain B, the Lupa Fault dominated the strain localization while the possible position of the southern termination of the Chisi shear zone (cf. Heilman et al., 2019; Lemna et al., 2019; Figs. Figs. 3A & 4) appears to have accommodated strains along rotated faulted blocks on the western side of the RRB (see Fig. 9C). This spatial arrangement implies that the Chisi shear zone crosscuts the Saza shear zone almost perpendicularly and implies the latter is sub-parallel to the RRB extension direction (cf. Figs. 3A & 4). We infer that the Saza shear zone extends into the RRB and continues sub-parallel to KSAZ (Figs. 3A) and ESE-striking faults (see Figs. 3A & 4). The Saza shear zone possibly provided an earlier strain shadow (cf. Reilly et al., 2017; Phillips et al., 2020) which inhibited an even distribution of regional stresses between the two structural domains, hence partitioning the extension rate and strains i.e. simultaneously higher extension and strain rate in Domain B than A.

In addition, the difference in the two structural domains may be attributable to segmentation and growth of the Lupa Fault (e.g. Withjack et al., 2002). The spatial distinctness of stratigraphy for each major unit in the two depocenters may be due to

existence of a large axial supply of sediment from the southeast where the nearest depocenter in Domain B became completely infilled before Domain A became progressively infilled (e.g. Withjack et al., 2002). Alternatively the differences may be attributable to climatic variation, lateral facies and provenance changes (cf. Mtelela et al., 2016).

Based on the present relative spatial position of the fault segments and their alignment along strike of the border faults i.e. inline versus en echelon segments (see Fig. 4), we infer that the Saza transfer fault segment most likely suggests a 'hard linkage' formed between two synthetic fault segments whose tips are offset. The Kwera transfer fault suggests a 'soft linkage' between overlapping discrete en-echelon normal fault segments (e.g. Nelson et al., 1992; Peacock and Parfitt, 2002; Delvaux et al., 2012; Zwaan et al., 2016; Heilman et al., 2019). A key observation is that no inversion structures are observed adjacent to the transfer faults or within the KSAZ (cf. Figs. 3A & 4). This suggests that this area formed a strain shadow, as commonly observed in transfer zones (e.g. Schlische, 1991; Lambiase and Bosworth 1995; McLeod et al., 2000). Similar features are identified in the Taranaki Basin, Farsund Basin, Gulf of Evvia and Gulf of Suez where the rift is divided into several depocenters separated by polarity changing transfer zones (e.g. Gawthorpe et al., 1990; Reilly et al., 2017; Phillips et al., 2020).

The overall deformation and structural patterns in the Rukwa Rift suggest oblique stresses dominated the extension in the Rukwa Rift in an ESE-WNW orientation (Fig. 3A). The mapped fault obliquity, orientations and patterns i.e. both the Karoo and post-Karoo faults, which largely penetrate the crystalline basement, would most likely occur when there was a pre-existing basement faults that were reactivated in an oblique divergent sense (cf. Peace et al., 2018; Figs. 3A & 4). However, the seismicity and geodetic observation reveal a complex kinematic interplay of the Nubia-Somalia-Rovuma-San plates near the Rukwa Rift (e.g. Saria et al., 2014; Stamps et al., 2018; Daly et al., 2020).

These tectonic plates and associated rift interactions may equally account for the temporal and spatial variations of the local resultant stresses in the Rukwa Rift, thus influencing the deformation described in this study (e.g. Walsh et al., 2001; Reilly et al., 2017; Fig. 3A).

5.2 Fault rotated fold styles

The occurrences of rotated fault propagation folds in the RRB suggest strain accommodation at the fault tip within the overlying synrift sedimentary package (e.g. Mitra, 1990; Fig. 11A-B). In the hanging wall of the normal faults, these sedimentary packages show rotational kinematics, most likely amplified by high rate of extension and folding above the uplifted footwall (e.g. Ravnås and Bondevik, 1997; Fig. 11A-B). These fold styles are most likely controlled by the presence of rheologically weak strata possibly pressurized shales in a stratigraphy, which impede direct strain accommodation during upward fault propagation (cf. Mitra, 1993; Couples et al., 1998; Withjack and Schlische, 2006; Ford et al., 2007; Hardy, 2018). We infer that the burial of a fault propagation tip implies that the sedimentation rate outpaced the incremental accommodation space generation during the Cretaceous - Pleistocene (e.g. Withjack et al., 2002; Fig. 11B).

In contrast to fault propagation folds discussed above, the fault propagation monoclines most likely reflect relatively slower rate of fault propagation with respect to the rate of fault displacement in asymmetrical trishear zones (cf. Jin and Groshong, 2006). Consequently, the fault propagation partitions the deformation into multilayer buckling, kink-band migration and limb rotations to form a wide monoclinal fold (cf. Mitra, 1990; Withajack et al., 1990; Hardy and McClay, 1999; Ferrill et al., 2004; Fig. 9D).

We hypothesise that for generation of fault bend folds in the RRB, fault initiation could have occurred at different depths and finally linking up i.e. deep - rooted basement faults

system which are gently dipping, linked up with the steeper faults in the overlying synrift strata both propagating upward at different rates (e.g. Fig. 11C-D). The Earthquake data from the Rukwa Rift indicate that the ruptures occur at varied depths between 25 and 35 km (Delvaux and Barth, 2010; Craig et al., 2011; Lavayssiere et al., 2019) thus, faults initiating at various depths could have merged, most likely the Ubendian shear zone in the underlying basement accelerating a more rotational fault geometry which we observe in Domain B (e.g. Osagiede et al., 2020; Fig. 11C-D). The fault bend geometries may trigger a reverse frictional drag as a passive response of synrift strata, which amplify folding in the hanging wall of the Lupa Fault (cf. Mitra, 1993; Withjack et al., 2002; Fig. 9B; Fig. 11D).

5.3 Inversion styles, mechanisms and timing

The earliest inversion structures mapped in the RRB exhibit multifaulted anticlines (Fig. 8B). We determine that this inversion affected only the Karoo Supergroup and the seismic data reveal that it occurred during Middle Mesozoic, possibly Early Jurassic times (cf. Fig. 8B). This phase was therefore before the deposition of the earliest Cretaceous Red Sandstone Group and just after the deposition of the Karoo Supergroup. We infer that, inversion was most likely attributable to compressional pulse associated with uplift during initiation of Gondwana rifting (e.g. Wopfner, 1993). This evidence precludes the argument that the transpressional inversion occurred during early Mesozoic as suggested by Delvaux et al. (2012).

The youngest inversion in the RRB was mild due to the absence of noticeable complete reversal of neither original normal faults displacement nor significant decrease in normal fault offsets. The synkinematic records observed suggest short-lived inversion phase during the Pleistocene affected the Lake Beds sequences in the uppermost stratigraphy (Fig. 10B). We infer that the variation of asymmetric and symmetric folds styles within both Domains A and B can be explained by the temporal and spatial variation of

mechanical properties of the stratigraphy and strain accommodation across the RRB (e.g. Withjack et al., 2002).

Our observations show that inversion anticlines are not uniformly distributed across the basin, with a significant absence of these structures in some areas and along other similar faults (cf. Fig. 4). Based on this observation, we suggest that, there may be strain shadows between faults and that the geometry of some faults acted as a buttress to far field regional and other resultant local forces where inversion only occurred on the larger and least geometrically complex segments of faults. (e.g. Walsh et al., 2001; Reilly et al., 2017; Phillips et al., 2020). Alternatively, the absence of inversion in some places may partly be attributable to steep dips, short wavelength folds and high density faulting not visible in 2D seismic reflection data (e.g. Morley et al., 1999a).

Within the EARS, such as the Lotikipi basin and the Anza Graben in Kenya, mild inversion occurred during the late Miocene-Pleistocene and has been linked to ridge push and spreading in the Red Sea and Gulf of Aden (Bott, 1991; Bosworth, 1992; Morley, 1999; Wescott et al., 1999). The spreading in the Red Sea and Gulf of Aden seems too remote to have been influenced the local strains in the Rukwa Rift and the whole Western branch of the EARS, rather we infer that this could possibly be explained by kinematic interactions of the Nubia-Victoria-Rovuma-San plates and associated tectonic boundaries occupied by rifts particularly the South Tanganyika, the North Malawi and the Southwestern (Luangwa) rifts (e.g. Saria et al., 2014; Lavayssière et al., 2019; Daly et al., 2020; Wedmore et al., 2021). These tectonic plates and associated rifts interaction could have induced a new stress regime and/or rotation leading to the inversion structures described in this study (e.g. Fig. 4). An alternative near-field mechanism is that inversion resulted from variation of resultant local strains on intrabasinal faults and complex inherited fabrics due to the multiphase tectonic history (e.g. Turner and Williams, 2004).

A final possibility is the presence of East African mantle plumes and localized magmatic pulses in the Rungwe Volcanic Province (Nyblade and Robinson, 1994), which are often associated with thermo-kinematic anomalies and might have induced local strain fields and rotation in the Rukwa Rift (cf. Negredo et al., 1995; Ziegler et al., 1995; Hansen and Nielsen, 2003). Further work is required to understand the mechanical and rheological complexities involved in these mechanisms, at the moment it is difficult to discern an exclusive single factor which caused inversion and explains its distribution particularly in the RRB.

5.4 Helium potential in the Rukwa Rift Basin

The Precambrian Basement beneath the RRB and the surrounding terranes are composed of mainly granitoids, gneisses and granulites which are rich in helium producing minerals, i.e uranium and thorium, and provide potential source rocks for radiogenic ^{4}He (Danabalan, 2017; Fig. 12A-D). An enhanced expulsion of ^{4}He and associated gases, such as nitrogen, is most likely triggered regionally by the onset of East African mantle plume activity and related rifting (e.g. Nyblade and Robinson, 1994; Ebinger and Sleep, 1998; Danabalan et al., 2021). The structural data presented here suggest that basement rooted faults trending NNW-SSE, NNE-SSW, NW-SE are linked to interconnected basement structures including Ubendian shear zones (e.g. Fig. 11D). The faults, fractures, shear zones, lithological contacts, porous and permeable strata are likely to provide the main conduits for migration of helium-nitrogen rich seeps in the RRB (cf. Fig. 3A; Fig. 8B; Fig. 11D; Fig. 12A-F). Notably the helium prospects in the RRB are preferentially located adjacent to both the Mbozi and the Lupa Terranes and exhibit a dense and deep - rooted structural heterogeneity, reactivated by polyphase tectonics (cf. Fig. 8B; Fig. 11A-B). Many other thermal springs sites are devoid of significant radiogenic helium concentration (e.g. Barry et al., 2013), possibly due to lack of fluid connectivity spatially, i.e. hydrothermal circulation of fluid carrying radiogenic helium and variability of crustal-scale open-system behaviour (e.g. Lowenstern et al., 2014).

Similar to hydrocarbon systems, the potential traps for helium in the RRB are either stratigraphic, structural or a combination of both (e.g. Gluyas and Swarbrick 2021). Potential stratigraphic traps in the RRB may include juxtaposition of the Karoo sequences leading to wedge truncation against the uplifted Precambrian Basement sealed by unconformity (cf. Fig. 7A-B; Fig. 8B). Within Domain B, the Upper Karoo Formation, Galula Formation and the Nsungwe Formation have been documented to comprise mainly sandstones with porosity between 16% and 28% (Roberts et al., 2010; Mtelela, 2016) hence they present potential reservoirs for helium accumulations (Fig. 12E). These strata exhibit extension related anticlines bound by unconformities (e.g. Fig. 2), which may provide an effective trap and seal (Fig. 12E).

The Lake Beds strata comprise siliciclastic sandstones with c.16% porosity (Mtelela et al., 2016), and thus may present fairly good reservoirs while the inversion anticlines identified in this interval may provide effective traps (Fig. 12E). Notably, shales and carbonates that have been documented in the Lake Beds strata (Mtelela, 2016) imply the presence of effective seals for helium. Analogue basins containing similar inversion anticlines, stratigraphy, and with proven recent hydrocarbon discoveries in the East African Rift System are the Albertine Graben in Uganda and the Turkana Basin (Kenya) (Morley et al., 1999a; Tiercelin et al., 2012; Abeinomugisha and Kasande, 2012). However given the small atomic radius of helium (e.g. Danabalan et al., 2021) and multiphase deformation, these helium traps may be at a greater risk of leakage and equally give rise to the surficial thermal springs rich in helium which are observed in the RRB (Fig. 8B-C; Fig. 12A).

The source of high nitrogen associated with helium-rich fluids in the RRB is still unclear. In this study we infer that previously documented organic rich shale and liptinite rich coals in the K2 unit in the Karoo Supergroup (Wescott et al., 1991; Kilembe and Rosendahl, 1992) might have undergone thermogenic reaction enhanced by rifting and

volcanic activity (e.g. Snyder et al., 2003; Williams et al., 1992). These events possibly resulted in nitrogen accumulations during the Cretaceous and Oligocene carbonatite volcanism and the recent Cenozoic Rungwe volcanism. During the catagenesis stage (80°-120°C), the thermogenic changes in the basin cause high NH_4^+ in pore fluids and substitution in potassic minerals i.e illites (Hunt, 1979; Paxton, 1984; Williams et al., 1992; Lawrence et al., 2021). This catagenesis stage coincides with the closure temperature of some helium retentive minerals e.g. apatite and hematite (Danabalan et al., 2021), which can possibly mix with nitrogen rich-carrier fluid and migrate with pristine ^4He from the crystalline basement into the Rukwa synrift strata (e.g. Fig. 12A-F). Depending on the reaction kinematics and bulk mineralogy, the NH_4^+ rich fluids may undergo anaerobic ammonia oxidation (anammox) enroute to surface to produce nitrogen gas (e.g. Williams et al., 1992; Strous et al., 1999). However, these inferences need to be tested by isotopic studies. Further from the highlands of the Rungwe volcanic centers, the admixture of hydrothermal fluids, meteoric water and mantle derived ^3He, provide the main advection recharge in the region and may dissolve other components i.e ^4He, carbonates enroute to relatively lowland Rukwa Rift Basin hence leading to binary mixture signatures for ^4He and ^3He across the region (Fig. 12A-F).

6.0 Conclusions

From this study we conclude;

- The overall deformation in the Rukwa Rift largely localizes on NW-striking border faults, intrabasinal faults (with NNE, NW and NNW-trends), shear zones and transfer zones. These structures accommodate ESE-WNW directed oblique

divergence and they exert control on accommodation space and occurrences of thermal springs rich in helium-nitrogen that are manifest at the surface regionally.

- The RRB exhibits a gently dipping wedge to a typical half-graben geometry containing synextensional sedimentary packages up to a maximum thickness of 6000 ms TWT. Within these sedimentary packages a series of anticline structures, mapped stratal juxtaposition and stratigraphic-unconformity are widely distributed in the basin, and provide potential subsurface traps for helium-rich fluids.
- The RRB exhibits both extensional and compressional fold styles i.e fault bend folds, fault propagation folds and fault propagation monocline which are collocated with the normal faults and are widely distributed within Domain A and B.
- The RRB exhibit two phases of inversion which resulted in different fold styles in the RRB; the first produced multifaulted anticlinal Karoo inversion during the Early Jurassic and the second was a mild and widespread inversion during the Pleistocene which gave rise to both symmetrical and asymmetrical open anticlines.
- The crystalline basement provides the source rocks for the radiogenic helium while nitrogen is derived from thermogenic reaction of organic rich shale and liptinite rich coals, enhanced by rifting and associated volcanic activity.

Acknowledgements

This work was funded by United Kingdom Commonwealth Scholarship Commission, the results of which is part of the first author's PhD study at Durham University. Tanzania Petroleum Development Corporation (TPDC) is thanked for providing the dataset. Authors are extending their gratitude to anonymous reviewers for critical reviews that significantly enhanced the output of this study.

Declaration of competing interests: Authors declare no conflict of interests.

Data availability statement

The data that support the findings of this study are available from Tanzania Petroleum Development Corporation (TPDC). Restrictions apply to the availability of these data, which were used under license for this study. Data are available from the author(s) with the permission of Tanzania Petroleum Development Corporation (TPDC).

Captions

Fig. 1 (A) Map showing the tectonic configuration and boundaries of the major plates i.e. the Nubia and Somalia plates and microplates including San, Victoria and Rovuma plates. The GPS vectors from the geodetic measurement (pink arrows) show relative rate of extension and direction extracted from Saria et al. (2014) along the Eastern and the Western branches of the EARS mapped on color-coded TanDEM-X 90m data (Fernandes et al., 2004; Saria et al., 2014; Stamps et al., 2018; Daly et al., 2020; Wedmore et al., 2021). (B) Close up map showing regional configuration of the tectonic plates and major rifts forming plate boundaries, superimposed on color-shaded terrain map. RVP=Rungwe Volcanic Province.

Fig. 2. Generalized stratigraphy of the Rukwa Rift Basin correlated with the major regional tectonic events, Formations (Fm), Unconformities (UC) and a synthetic seismogram generated from well logs i.e. the bulk density and acoustic logs tied to seismic section (TVZ-26). Stratigraphic data (well tops information) from the geological report are correlated with high amplitude seismic horizons, hence providing confidence and control during interpretation. The ages of key horizons are constrained using previous work by Mtelela, (2016); Hilbert-Wolf et al., 2017; Lawrence et al., 2021 and references therein. Sup = Supergroup; Gr = Group; NFT = Nsungwe Formation Tuffs.

Fig. 3. (A) Map showing the Precambrian terranes surrounding the Rukwa Rift Basin with rose diagrams that summarise the main lineaments trends showing NW-SE, NNW-SSE and NNE-SSW directions, mapped on hill shade images. The intrabasinal faults are interpreted from seismic data. The Mbozi Block bifurcates the basin into the Musongano trough (MST) to the West and the Songwe sub-basin (SNT) to the east. Note the shear zones separating different terranes i.e Mughese, Mtose, Chisi and Saza shear zones (e.g. Mnali, 1999; Heilman et al., 2019; Lemna et al., 2019; Kolawole et al., 2021). Note the Saza shear zone lies sub-parallel to the extension direction and perpendicular to the Chisi shear zone. Cross sections (B-B′ and C-C′) show the general basin geometry in Domain A and B respectively, separated by the Kwera-Saza Accommodation Zone (KSAZ) (see Fig. 4 for domain locations).

Fig. 4. Time-thickness map for the Lake Beds Group superimposed on hill shaded map and interpreted structures showing intrabasinal faults, distribution of inversion structures and depocenters segmented into Domain A and B. Note the WNW-ESE – striking faults perpendicular to the Chisi Shear Zone (CSZ) and sub-parallel to the Saza Shear Zone (SSZ).

Fig. 5. (A) Geoseismic sections interpreted within Domain A characterized by uniformly steep Lupa Fault and, asymmetrical and symmetrical folds. (B) Seismic section showing symmetrical folds (white curves) bounded by steeply dipping conjugate normal faults in the middle and western part of the basin. (C) Seismic section showing symmetrical folds (white curve) associated with the antithetic faults within proximity of c. 5 - 10 km from the Lupa Fault (D) Sketch map showing the location of seismic lines illustrated in Figs. 5 & 6 in relation to the position of the Lake Rukwa (See also Fig. 9A for map location).

Fig. 6. Geoseismic section through Domain B of the RRB showing the temporal stratigraphic distribution of a typical half-graben geometry. The synrift sediment packages dip steeply towards the rotated Lupa Fault and thin up to surface on top of the

uplifted Mbozi block. Note the Lower Karoo Formation characterized by basement-rooted faults, which are truncated at top Lower Karoo horizon (see Fig. 5D & 9A for map location).

Fig. 7. (A) Uninterpreted seismic section. (B) Interpreted geosection illustrating the topographic basement high, truncation of Karoo strata and unconformity associated with strong amplitude response. Note the NE trending fault (NW and SE-dipping) is located adjacent to Kwera relay ramp (see Fig. 4 and Fig. 9A for map view and location).

Fig. 8. (A) A map showing location of thermal springs in the basin, lithology distribution after Mtelela, (2016) and 2D seismic section trace in vicinity of Ivuna and Itumbula shown by the purple line B - B′. (B) A series of rotated faulted blocks associated with strata juxtaposition of both Karoo and Red Sandstone. Note the inverted Karoo Supergroup at SW end. (C) A photo showing bubbles of nitrogen dominated helium-rich rich gas from Ivuna salt pan associated with thermal saline surface seeps. The photo was taken viewing north adjacent to basement outcrops. The location of the cross section is shown by the purple line B-B′ and sample sites for helium shown in a triangular blue symbols numbered from 1-7 in Fig. 8A (see geochemical details for each site in Table 2).

Fig. 9. (A) A map showing the surface location of the interpreted seismic sections indicated by purple thick lines. (B) Geoseismic section showing the fault bend folds as a passive response due to bending/rotation in the geometry of the Lupa Fault. (C) Interpreted seismic section showing faulted block rotation and fault propagation folds. Note the syn-kinematic record of onlaps in the Lake Beds sequences and propagating fault tip in the NE end, buried due to high sedimentation rate. (D) Breached fault propagation monocline with anticline in the footwall and syncline in the hanging wall. Note the rotated Lake Beds strata in the lower section due to space accommodation during fault propagation whereas the uppermost strata are inverted.

Fig. 10. (A) Interpreted geoseismic section illustrating inversion styles i.e symmetrical and asymmetrical anticline inversion within steeply dipping faults. (B) Close up of interpreted seismic section showing symmetrical folds inversions styles between the high angle faults. Note the synkinematic sediment onlaps revealing the timing of inversion (Pleistocene age). (See Fig. 9A for map location).

Fig. 11 (A) Geological section showing gently dipping synrift sedimentary packages created during Late Carboniferous to Permian times. (B) Fault propagation folding and strata rotation amplified by folding and high extension rate during Cretaceous-Pleistocene. (C) Deeper gently-dipping fault and shallower steeply-dipping Lupa fault both propagating upward at different rates. (D) Merging of newly forming faults from crystalline basement which propagates upward interacting with a shallower propagating Lupa Fault resulting into fault bend and reverse drag of strata to form folds in the hanging wall.

Fig. 12. (A) Cross section showing the generalized thermal fluid system associated with helium in the Rukwa Rift Basin. (B) Mantle derived ^{3}He associated with high CO_2 outgassing from the Rungwe Volcanic Province (Barry et al., 2013; Danabalan, 2017). (C) Secondary migration involving binary mixing between a pure crustal end member and a mantle end member i.e. high ^{4}He concentrations, associated high N_2 concentrations and low $^{3}He/^{4}He$ ratios (predominantly crustal input) whereas closer to the Rungwe Volcanic Province high CO_2, low N_2, low ^{4}He and high $^{3}He/^{4}He$ ratios (mantle input) observed by Barry et al. (2013) and Danabalan, (2017). (D) Primary migration of ^{4}He involving diffusion from helium producing minerals at high temperature above the closure temperature and interconnected fractures due to overpressure (Warr et al., 2018; Danabalan et al., 2021). (E) Potential traps for helium involving inverted Lake Beds strata and relatively older monocline traps sealed by unconformities. (F) A photo taken facing

NE at the Lupa Fault showing that the thermal spring systems clearly follow the lithology contacts, faults and fracture network systems.

References

Abeinomugisha, D. and Kasande, R., 2012. Tectonic control on hydrocarbon accumulation in the intracontinental Albertine Graben of the East African rift system. AAPG International Conference and Exhibition, Cape Town, South Africa, October 26-29, 2008.

Allmendinger, R. W., Cardozo, N. C., and Fisher, D., 2013. Structural Geology Algorithms: Vectors & Tensors: Cambridge, England, Cambridge University Press, 289 pp.

Avseth, P., Mukerji, T. and Mavko, G., 2010. Quantitative seismic interpretation: Applying rock physics tools to reduce interpretation risk. Cambridge university press.

Barry, P. H., Hilton, D. R., Fischer, T. P., De Moor, J. M., Mangasini, F., & Ramirez, C., 2013. Helium and carbon isotope systematics of cold "mazuku" CO2 vents and hydrothermal gases and fluids from Rungwe Volcanic Province, southern Tanzania Chemical Geology, 339, 141-156. https://doi.org/10.1016/j.chemgeo.2012.07.003.

Boniface, N., Schenk, V., and Appel, P., 2012. Paleoproterozoic eclogites of MORB-type chemistry and three Proterozoic orogenic cycles in the Ubendian Belt (Tanzania): Evidence from monazite and zircon geochronology, and geochemistry. Precambrian Research, 192,16–33 https://doi.org/10.1016/j.precamres.2011.10.007.

Bosworth, W., 1992. Mesozoic and early Tertiary rift tectonics in East Africa. *Tectonophysics*, *209*(1-4), pp.115-137.

Bott, M.H.P., 1991. Ridge push and associated plate interior stress in normal and hot spot regions. *Tectonophysics*, *200*(1-3), pp.17-32.

Chorowicz, J. and Mukonki, M.B., 1980. Lineaments anciens, zones transformantes recentes et geotectoniques des fosses dans l'est African, d'après la teledetection et la microtectonique: Museum Royal Africa Central, Tervuren, Belgium. Department of Geology and Mineralogy Annual Report, pp. 143–146.

Chorowicz, Jean, 2005. "The East African rift system". Journal of African Earth Sciences. **43** (1):

379–410. https://doi.org/10.1016/j.jafrearsci.2005.07.019.

Couples, G.D., Lewis, H. and Tanner, P.G., 1998. Strain partitioning during flexural-slip folding. Geological Society, London, Special Publications, 127(1), pp.149-165. https://doi.org/10.1144/GSL.SP.1998.127.01.12

Craig, T.J., Jackson, J.A., Priestley, K. and McKenzie, D., 2011. Earthquake distribution patterns in Africa: their relationship to variations in lithospheric and geological structure, and their rheological implications. *Geophysical Journal International*, *185*(1), pp.403-434.

Daly, M.C., Green, P., Watts, A.B., Davies, O., Chibesakunda, F. and Walker, R., 2020. Tectonics and landscape of the Central African Plateau and their implications for a propagating Southwestern Rift in Africa. *Geochemistry, Geophysics, Geosystems*, *21*(6), p.e2019GC008746.

Daly, M. C, 1988. Crustal shear zones in central Africa—A kinematic approach to Proterozoic tectonics. Episodes, 11(1), 5–11. https://doi.org/10.18814/epiiugs/1988/v11i1/003.

Daly, M.C., Chorowicz, J., Fairhead, J.D., 1989. Rift basin evolution in Africa: the influence of reactivated steep basement shear zones. Geological Society, London, Special Publications 44, 309. https://doi.org/10.1144/GSL.SP.1989.044.01.17.

Danabalan, D., 2017. Helium: Exploration Methodology for a Strategic Resource. PhD Thesis, Durham University.

Danabalan, D., Gluyas, J., Macpherson, C.G, Abraham-James, T.H, Bluett, J.J, Barry, P.H, and Ballentine, C.J, 2021. Principles of Helium Exploration. *Petroleum Geoscience* (In press).

Delvaux, D., Levi, K., Kajara, R., & Sarota, J., 1992. Cenozoic paleostress and kinematic evolution of the Rukwa–North Malawi rift valley (East African Rift System). Bulletin des Centres de Recherche Exploration-Production ElfAquitaine, 16, 383–406.

Delvaux, D., 2001. Karoo rifting in western Tanzania: precursor of Gondwana break-up. *Contributions to geology and paleontology of Gondwana in honor of Helmut Wopfner: Cologne, Geological Institute, University of Cologne*, pp.111-125.

Delvaux, D. and Barth, A., 2010. African stress pattern from formal inversion of focal mechanism data. *Tectonophysics*, *482*(1-4), pp.105-128.

Delvaux, D., Kervyn, F., Macheyeki, A. S., & Temu, E. B., 2012. Geodynamic significance of the TRM segment in the East African Rift (W-Tanzania): Active tectonics and paleostress in the Ufipa plateau and Rukwa basin. Journal of Structural Geology, 37, 161–180.

https://doi.org/10.1016/j.jsg.2012.01.008.

Delvaux, D., Kraml, M., Sierralta, M., Wittenberg, A., Mayalla, J.W., Kabaka, K., Makene, C. and GEOTHERM Working Group, 2010. Surface Exploration of a Viable Geothermal Resource in Mbeya Area, Sw Tanzania. Part I: Geology of the Ngozi-Songwe Geothermal System.

Ebinger, C.J., 1989. Tectonic development of the western branch of East African rift system. Geol. Soc. Am. Bull. 101, 885-903. https://doi.org/10.1130/0016-7606(1989)101%3C0885:TDOTWB%3E2.3.CO2.

Ebinger, C.J., Deino, A.L., Drake, R.E. and Tesha, A.L., 1989. Chronology of volcanism and rift basin propagation: Rungwe volcanic province, East Africa. *Journal of Geophysical Research: Solid Earth*, *94*(B11), pp.15785-15803. https://doi.org/10.1029/JB094iB11p15785.

Ebinger, C., and N. H. Sleep.,1998. Cenozoic magmatism in central and east Africa resulting from impact of one large plume, Nature, 395, 788-791.

Ebinger, Cynthia, 2005. "Continental break-up: The East African perspective". Astronomy and Geophysics. 46 (2): 2.16–2.21. https://doi.org/10.1111/j.1468-4004.2005.46216.x.

Fernandes, R.M.S., Ambrosius, B.A.C., Noomen, R., Bastos, L., Combrinck, L., Miranda, J.M. and Spakman, W., 2004. Angular velocities of Nubia and Somalia from continuous GPS data: implications on present-day relative kinematics. *Earth and Planetary Science Letters*, *222*(1), pp.197-208.

Ferrill, D.A., Morris, A.P., Sims, D.W., Waiting, D.J., Hasegawa, S., 2004. Development of synthetic layer dip adjacent to normal faults. In: Sorkhabi, R., Tsuji, Y. (Eds.), Faults, Fluid Flow, and Petroleum Traps American Association of Petroleum Geologists Memoir. American Association of Petroleum Geologists, Tulsa, OK, USA, pp. 125–138. DOI:10.1306/1033720M853133.

Ford, M., De Veslud, C.L.C. and Bourgeois, O., 2007. Kinematic and geometric analysis of fault-related folds in a rift setting: The Dannemarie basin, Upper Rhine Graben, France. Journal of Structural Geology, 29(11), pp.1811-1830. https://doi.org/10.1016/j.jsg.2007.08.001.

Fritz, H., Abdelsalam, M., Ali, K. A., Bingen, B., Collins, A. S., Fowler, A. R., et al. (2013). Orogen styles in the East African Orogen: Areview of the Neoproterozoic to Cambrian tectonic evolution. Journal of African Earth Sciences, 86, 65–106. https://doi.org/10.1016/j.jafrearsci.2013.06.004.

Gawthorpe, R.L., Hurst, J.M. and Sladen, C.P., 1990. Evolution of Miocene footwall-derived coarse-grained deltas, Gulf of Suez, Egypt: implications for exploration. *AAPG bulletin*, *74*(7), pp.1077-1086.

Gawthorpe, R.L. and Hurst, J.M., 1993. Transfer zones in extensional basins: their structural style and influence on drainage development and stratigraphy. *Journal of the Geological Society*, *150*(6), pp.1137-1152. https://doi.org/10.1144/gsjgs.150.6.1137.

Gluyas, J.G. and Swarbrick, R.E., 2021. *Petroleum geoscience*. John Wiley & Sons.

Jin, G. and Groshong Jr, R.H., 2006. Trishear kinematic modeling of extensional fault-propagation folding. *Journal of Structural Geology*, *28*(1), pp.170-183. https://doi.org/10.1016/j.jsg.2005.09.003.

Hansen, D.L. and Nielsen, S.B., 2003. Why rifts invert in compression. *Tectonophysics*, *373*(1-4), pp.5-24. https://doi.org/10.1016/S0040-1951(03)00280-4.

Hardy, S., 2018. Coupling a frictional- rifts invert in compression cohesive cover and a viscous substrate in a discrete element model: First results of application to thick-and thin-skinned extensional tectonics. *Marine and Petroleum Geology*, *97*, pp.32-44. https://doi.org/10.1016/j.marpetgeo.2018.06.026.

Hardy, S., McClay, K., 1999. Kinematic modeling of extensional fault propagation folding. Journal of Structural Geology 21, 695–702. https://doi.org/10.1016/S0191-8141(99)00072-3

Heilman, E., Kolawole, F., Atekwana, E. A., & Mayle, M., 2019. Controls of basement fabric on the linkage of rift segments. *Tectonics*, 38, 1337–1366. https://doi.org/10.1029/2018TC005362.

Hayward, A. B., and Graham, R. H., 1989. Some geometrical characteristics of inversion. *Geological Society, London, Special Publications*, *44*(1), 17-39. https://doi.org/10.1144/GSL.SP.1989.044.01.03.

Hilbert-Wolf, H., Roberts, E., Downie, B., Mtelela, C., Stevens, N.J. and O'Connor, P., 2017. Application of U–Pb detrital zircon geochronology to drill cuttings for age control in hydrocarbon exploration wells: A case study from the Rukwa Rift Basin, Tanzania. *AAPG Bulletin*, *101*(2), pp.143-159.

Holland, G., Lollar, B. S., Li, L., Lacrampe-Couloume, G., Slater, G. F., & Ballentine, C. J., 2013. Deep fracture fluids isolated in the crust since the Precambrian era. *Nature*, *497* (7449), 357.

Hunt, J. M., 1979. Petroleum Geochemistry and Geology. W. H. Freeman.

James, T. C.,1967a. Thermal springs in Tanzania. *Institution of Mining and Metallurgy*, Transactions/Section B (Applied Earth Science) 76, B1–B18 *in* Macheyeki, A. S., Delvaux, D., De Batist, M., & Mruma, A. (2008). Fault kinematics and tectonic stress in the seismically active Manyara–Dodoma Rift segment in Central Tanzania–Implications for the East African Rift. *Journal of African Earth Sciences*, *51*(4), 163-188.

James, T. C., 1967b. Thermal springs in Tanzania – discussions and conclusions. *Institution of Mining and Metallurgy*, Transactions/Section B (Applied Earth Science) 76, B168–B174 *in* Macheyeki, A. S., Delvaux, D., De Batist, M., & Mruma, A. (2008). Fault kinematics and tectonic stress in the seismically active Manyara–Dodoma Rift segment in Central Tanzania–Implications for the East African Rift. *Journal of African Earth Sciences*, *51*(4), 163-188.

Katumwehe, A. B., Abdelsalam, M. G., & Atekwana, E. A., 2015. The role of pre-existing Precambrian structures in rift evolution: The Albertine and Rhino grabens, Uganda. Tectonophysics, 646, 117–129. https://doi.org/10.1016/j.tecto.2015.01.022.

Kervyn, F., Ayub, S., Kajara, R., Kanza, E., & Temu, B., 2006. Evidence of recent faulting in the Rukwa rift (West Tanzania) based on radar interferometric DEMs. *Journal of African Earth Sciences*, *44*(2), 151-168. https://doi.org/10.1016/j.jafrearsci.2005.10.008.

Kilembe, E. A., & Rosendahl, B. R., 1992. Structure and stratigraphy of the Rukwa rift. *Tectonophysics*, *209*(1-4), 143-158.

Kolawole, F., Phillips, T.B., Atekwana, E.A. and Jackson, C.A.L., 2021. Structural inheritance controls strain distribution during early continental rifting, Rukwa Rift. *Frontiers in Earth Science*, p.670. https://doi.org/10.3389/feart.2021.707869

Lambiase, J.J. and Bosworth, W., 1995. Structural controls on sedimentation in continental rifts. *Geological Society, London, Special Publications*, *80*(1), pp.117-144. https://doi.org/10.1144/GSL.SP.1995.080.01.06.

Lawrence, L., Spandler, C., Roberts, E.M. and Hilbert-Wolf, H.L., 2021. Mineralogy and origin of the alkaline Nsungwe Formation tuffs of the Rukwa Rift Basin, southwestern Tanzania. *Lithos*, *380*, p.105885.

Lavayssière, A., Drooff, C., Ebinger, C., Gallacher, R., Illsley-Kemp, F., Oliva, S.J. and Keir, D., 2019. Depth extent and kinematics of faulting in the southern Tanganyika rift, Africa. *Tectonics*, *38*(3), pp.842-862.

Lemna, O. S., Stephenson, R., & Cornwell, D. G., 2019. The role of pre-existing Precambrian structures in the development of Rukwa RiftBasin, southwest Tanzania. Journal of African Earth Sciences, 150, 607–625.

Lenoir, J.L., Liégeois, J.P., Theunissen, K. and Klerkx, J., 1994. The Palaeoproterozoic Ubendian shear belt in Tanzania: geochronology and structure. *Journal of African Earth Sciences*, *19*(3), pp.169-184.

Lowenstern, J.B., Evans, W.C., Bergfeld, D. and Hunt, A.G., 2014. Prodigious degassing of a billion years of accumulated radiogenic helium at Yellowstone. *Nature*, *506*(7488), pp.355-358.

Mbede, E.I., 1993. Tectonic development of the Rukwa Rift basin in SW Tanzania (Vol. 152). Fachber. Geowiss., TU Berlin.

Mitra, S., 1990. Fault-propagation folds: geometry, kinematic evolution, and hydrocarbon traps. *AAPG bulletin*, *74*(6), pp.921-945.

Mitra, S., 1993. Geometry and kinematic evolution of inversion structures. *AAPG Bulletin*, *77*(7), pp.1159-1191. https://doi.org/10.1306/BDFF8E2A-1718-11D7-8645000102C1865D.

McLeod, A.E., Dawers, N.H. and Underhill, J.R., 2000. The propagation and linkage of normal faults: insights from the Strathspey–Brent–Statfjord fault array, northern North Sea. *Basin Research*, *12*(3-4), pp.263-284. https://doi.org/10.1111/j.1365-2117.2000.00124.x.

Mnali, S.R., 1999. Palaeoproterozoic felsic magmatism and associated gold-quartz vein mineralization in the western part of the Lupa goldfield, south-western Tanzania. Unpublished PhD thesis, University of Dar es Salaam, Tanzania, 198 p.

Morley, C. K., R. M. Harper and S. T. Wigger., 1999a. Tectonic Inversion in East Africa, in C. K. Morley ed., Geoscience of Rift Systems – Evolution of East African Rift System: AAPG studies in Geology No. 44, p. 193-210.

Morley, C.K., R.A. Day, R. Lauck, R. Bosher, D.M. Stone, S.T. Wigger, W.A. Wescott, D. Haun, N. Bassett, and W. Bosworth., 1999b. Geology and Geophysics of the Anza Graben, in C.K. Morley ed., Geoscience of Rift Systems—Evolution of East Africa: *AAPG Studies in Geology* No. 44, p. 67–90.

Morley, C.K., Cunningham, S.M., Harper, R.M. and Wescott, W.A., 1992. Geology and geophysics of the Rukwa rift, East Africa. *Tectonics*, *11*(1), pp.69-81.

Morley, C.K., 1989, Extension, detachments, and sedimentation in continental rifts (with

particular reference to East Africa): Tectonics, v. 8, p. 1175–1192.

Morley, C.K. ed., 1999. *Geoscience of rift systems: evolution of East Africa* (No. 44). Amer Assn of Petroleum Geologists.

Mtelela, C., Roberts, E.M., Hilbert-Wolf, H.L., Downie, R., Hendrix, M.S., O'Connor, P.M. and Stevens, N.J., 2017. Sedimentology and paleoenvironments of a new fossiliferous late Miocene-Pliocene sedimentary succession in the Rukwa Rift Basin, Tanzania. *Journal of African Earth Sciences*, *129*, pp.260-281.

Mtelela, C., 2016. Sedimentology and stratigraphy of the late Cenozoic lake beds succession, Rukwa Rift Basin, Tanzania: implications for hydrocarbon prospectivity (Doctoral dissertation, James Cook University). https://researchonline.jcu.edu.au/47290/.

Mtelela, C., Roberts, E.M., Downie, R. and Hendrix, M.S., 2016. Interplay of structural, climatic, and volcanic controls on late quaternary lacustrine–deltaic sedimentation patterns in the Western Branch of the East African Rift System, Rukwa Rift Basin, Tanzania. *Journal of Sedimentary Research*, *86*(10), pp.1179-1207.

Negredo, A.M., Fernandez, M. and Zeyen, H., 1995. Thermo-mechanical constraints on kinematic models of lithospheric extension. *Earth and Planetary Science Letters*, *134*(1-2), pp.87-98. https://doi.org/10.1016/0012-821X(95)00107-N.

Nelson, R.A., Patton, T.L. and Morley, C.K., 1992. Rift-segment interaction and its relation to hydrocarbon exploration in continental rift systems (1). *AAPG bulletin*, *76*(8), pp.1153-1169. https://doi.org/10.1306/BDFF898E-1718-11D7-8645000102C1865D.

Nyblade, A.A. and Robinson, S.W., 1994. The African superswell. *Geophysical research letters*, *21*(9), pp.765-768.

Osagiede, E.E., Rotevatn, A., Gawthorpe, R., Kristensen, T.B., Jackson, C.A. and Marsh, N., 2020. Pre-existing intra-basement shear zones influence growth and geometry of non-colinear normal faults, western Utsira High–Heimdal Terrace, North Sea. *Journal of Structural Geology*, *130*, p.103908.

Paxton, S. T., 1984. Occurrence and distribution of am- monium illite in the Pennsylvania, U.S.A. coal fields and proposed relationship to thermal maturity. Geol. Soc. Am. Abstr. Prog. 16,620.

Peace, A., McCaffrey, K., Imber, J., van Hunen, J., Hobbs, R. and Wilson, R., 2018. The role of pre-existing structures during rifting, continental breakup and transform system

development, offshore West Greenland. *Basin Research*, *30*(3), pp.373-394. https://doi.org/10.1111/bre.12257.

Peacock, D.C.P., Parfitt, E.A., 2002. Active relay ramps and normal fault propagation on Kilauea Volcano, Hawaii. Journal of structural geology 24, 729e742. https://doi.org/10.1016/S0191-8141(01)00109-2.

Phillips, T., Jackson, C. A. L., and Norcliffe, J., 2020. Pre-inversion normal fault geometry controls inversion style and magnitude, Farsund Basin, offshore southern Norway. *Solid Earth*. https://doi.org/10.5194/se-11-1489-2020.

Quennell, A.M., McKinlay, A.C. and Aitken, W.G., 1956. Summary of the geology of Tanganyika, part 1. *Geological Surv. Tanganyika Mem*, *126*.

Ravnås, R., & Bondevik, K.,1997. Architecture and controls on Bathonian–Kimmeridgian shallow-marine synrift wedges of the Oseberg–Brage area, northern North Sea. *Basin Research*, *9*(3), 197-226.

Reilly, C., Nicol, A. and Walsh, J., 2017. Importance of pre-existing fault size for the evolution of an inverted fault system. *Geological Society, London, Special Publications*, *439*(1), pp.447-463. https://doi.org/10.1144/SP439.2.

Rizzoli, P., Martone, M., Gonzalez, C., Wecklich, C., Tridon, D.B., Bräutigam, B., Bachmann, M., Schulze, D., Fritz, T., Huber, M. and Wessel, B., 2017. Generation and performance assessment of the global TanDEM-X digital elevation model. *ISPRS Journal of Photogrammetry and Remote Sensing*, *132*, pp.119-139. https://elib.dlr.de/113892/.

Roberts, E.M., Stevens, N.J., O'Connor, P.M., Dirks, P.H.G.M., Gottfried, M.D., Clyde, W.C., Armstrong, R.A., Kemp, A.I.S. and Hemming, S., 2012. Initiation of the western branch of the East African Rift coeval with the eastern branch. *Nature Geoscience*, *5*(4), pp.289-294.

Roberts, E.M., O'Connor, P.M., Stevens, N.J., Gottfried, M.D., Jinnah, Z.A., Ngasala, S., Choh, A.M. and Armstrong, R.A., 2010. Sedimentology and depositional environments of the Red Sandstone Group, Rukwa Rift Basin, southwestern Tanzania: New insight into Cretaceous and Paleogene terrestrial ecosystems and tectonics in sub-equatorial Africa. *Journal of African Earth Sciences*, *57*(3), pp.179-212. https://doi.org/10.1016/j.jafrearsci.2009.09.002.

Roe, E., Dypvik, H. and Kilembe, E., 1996. Sedimentological analysis of the logs and cuttings from the wells Ivuna #1 and Galula #1, the Rukwa Rift valley, Western Tanzania- A progress report

(Unpublished).

Rosendahl, B.R., Reynolds, D.J., Lorber, P.M., Burgess, C.F., McGill, J., Scott, D., Lambiase, J.J. and Derksen, S.J., 1986. Structural expressions of rifting: lessons from Lake Tanganyika, Africa. *Geological Society, London, Special Publications*, *25*(1), pp.29-43.

Sander, S. and Rosendahl, B.R., 1989. The geometry of rifting in Lake Tanganyika, east Africa. *Journal of African Earth Sciences (and the Middle East)*, *8*(2-4), pp.323-354.

Saria, E., Calais, E., Stamps, D. S., Delvaux, D., & Hartnady, C. J. H. , 2014. Present-day kinematics of the East African Rift. Journal of Geophysical Research: Solid Earth, 119, 3584–3600. https://doi.org/10.1002/2013JB010901.

Schlische, R.W., 1991. Half-graben basin filling models: new constraints on continental extensional basin development. *Basin Research*, *3*(3), pp.123-141. https://doi.org/10.1111/j.1365-2117.1991.tb00123.x.

Smets, B., Delvaux, D., Ross, K.A., Poppe, S., Kervyn, M., d'Oreye, N. and Kervyn, F., 2016. The role of inherited crustal structures and magmatism in the development of rift segments: Insights from the Kivu basin, western branch of the East African Rift. *Tectonophysics*, *683*, pp.62-76.

Snyder, G., Poreda, R., Fehn, U. and Hunt, A., 2003. Sources of nitrogen and methane in Central American geothermal settings: Noble gas and 129I evidence for crustal and magmatic volatile components. *Geochemistry, Geophysics, Geosystems*, *4*(1), pp.1-28.

Stamps, D.S., Saria, E. and Kreemer, C., 2018. A geodetic strain rate model for the East African Rift System. *Scientific reports*, *8*(1), pp.1-9. DOI:10.1038/s41598-017-19097-w

Strous, M., Fuerst, J.A., Kramer, E.H., Logemann, S., Muyzer, G., van de Pas-Schoonen, K.T., Webb, R., Kuenen, J.G. and Jetten, M.S., 1999. Missing lithotroph identified as new planctomycete. *Nature*, *400*(6743), pp.446-449.

Theunissen, K., Klerkx, J., Melnikov, A., & Mruma, A., 1996. Mechanisms of inheritance of rift faulting in the western branch of the East African Rift, Tanzania. *Tectonics*, *15*(4), 776-790. https://doi.org/10.1029/95TC03685.

Tiercelin, J.J., Thuo, P., Potdevin, J.L. and Nalpas, T., 2012. Hydrocarbon prospectivity in Mesozoic and early–middle Cenozoic rift basins of central and northern Kenya, Eastern Africa. DOI:10.1306/13351553M1001742.

Turner, J.P. and Williams, G.A., 2004. Sedimentary basin inversion and intra-plate shortening. *Earth-Science Reviews*, *65*(3-4), pp.277-304.

Walsh, J.J. and Watterson, J., 1989. Displacement gradients on fault surfaces. *Journal of Structural Geology*, *11*(3), pp.307-316.

Walsh, J.J., Childs, C., Meyer, V., Manzocchi, T., Imber, J., Nicol, A., Tuckwell, G., Bailey, W.R., Bonson, C.G., Watterson, J. and Nell, P.A., 2001. Geometric controls on the evolution of normal fault systems. *Geological Society, London, Special Publications*, *186*(1), pp.157-170. https://doi.org/10.1144/GSL.SP.2001.186.01.10.

Warr, O., Lollar, B.S., Fellowes, J., Sutcliffe, C.N., McDermott, J.M., Holland, G., Mabry, J.C. and Ballentine, C.J., 2018. Tracing ancient hydrogeological fracture network age and compartmentalisation using noble gases. *Geochimica et Cosmochimica Acta*, *222*, pp.340-362.

Wedmore, L.N., Biggs, J., Floyd, M., Fagereng, Å., Mdala, H., Chindandali, P., Williams, J.N. and Mphepo, F., 2021. Geodetic constraints on cratonic microplates and broad strain during rifting of thick Southern African lithosphere. *Geophysical Research Letters*, *48*(17), p.e2021GL093785. https://doi.org/10.1029/2021GL093785.

Wescott, W.A., S.T. Wigger, D.M. Stone, and C.K. Morley., 1999, Geology and Geophysics of the Lotikipi Plain, in C.K. Morley ed., Geoscience of Rift Systems—Evolution of East Africa: *AAPG Studies in Geology No*. 44, p. 55–65.

Wescott, W.A., W.N. Krebs, D.W. Englehardt, and S.M. Cunningham, 1991, New biostratigraphic age dates from the Lake Rukwa basin in western Tanzania: AAPG Bulletin, v.75, p. 1255–1263.

Wessel, B., 2016. TanDEM-X Ground Segment DEM Products Specification Document. Technical Note 3.1, German Aerospace Center (DLR). https://tandemx-science.dlr.de/

Wheeler,W.H. & Rosendahl, B.R., 1994. Geometry of the Livingstone Mountains Border-fault, Nyasa (Malawi) Rift, East Africa.Tectonics, 13, 303-312. https://doi.org/10.1029/93TC02314.

Widlansky, S.J., Clyde, W.C., O'connor, P.M., Roberts, E.M. and Stevens, N.J., 2018. Paleomagnetism of the Cretaceous Galula Formation and implications for vertebrate evolution. *Journal of African Earth Sciences*, *139*, pp.403-420.

Williams, L.B., Wilcoxon, B.R., Ferrell, R.E. and Sassen, R., 1992. Diagenesis of ammonium during hydrocarbon maturation and migration, Wilcox Group, Louisiana, USA. *Applied*

Geochemistry, *7*(2), pp.123-134.

Withjack, M.O., Schlische, R.W. and Olsen, P.E., 2002. Rift-basin structure and its influence on sedimentary systems. DOI: 10.2110/pec.02.73.0057.

Withjack, M.O. and Schlische, R.W., 2006. Geometric and experimental models of extensional fault-bend folds. *Geological Society, London, Special Publications*, *253*(1), pp. 285-305. https://doi.org/10.1144/GSL.SP.2006.253.01.15.

Wopfner, H., 1993. Structural development of Tanzanian Karoo basins and the break-up of Gondwana. In *Gondwana symposium* (pp. 531-539).

Ziegler, P.A., Cloetingh, S. and van Wees, J.D., 1995. Dynamics of intra-plate compressional deformation: the Alpine foreland and other examples. *Tectonophysics*, *252*(1-4), pp.7-59. https://doi.org/10.1016/0040-1951(95)00102-6.

Zink, M., Bachmann, M., Brautigam, B., Fritz, T., Hajnsek, I., Moreira, A., Wessel, B. and Krieger, G., 2014. TanDEM-X: The new global DEM takes shape. *IEEE Geoscience and Remote Sensing Magazine*, *2*(2), pp.8-23.

Zwaan, F., Schreurs, G., Naliboff, J. and Buiter, S.J., 2016. Insights into the effects of oblique extension on continental rift interaction from 3D analogue and numerical models. *Tectonophysics*, 693, pp.239-260. https://doi.org/10.1016/j.tecto.2016.02.036.

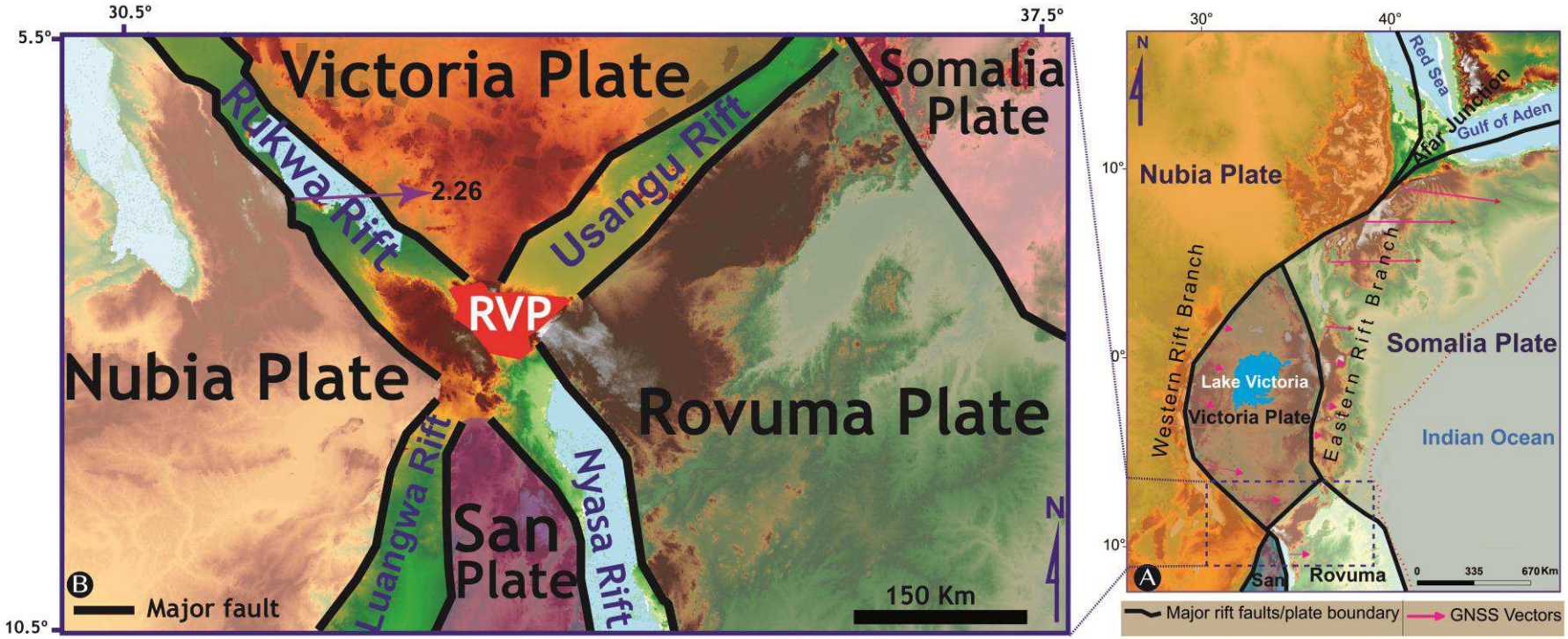

Fig. 1

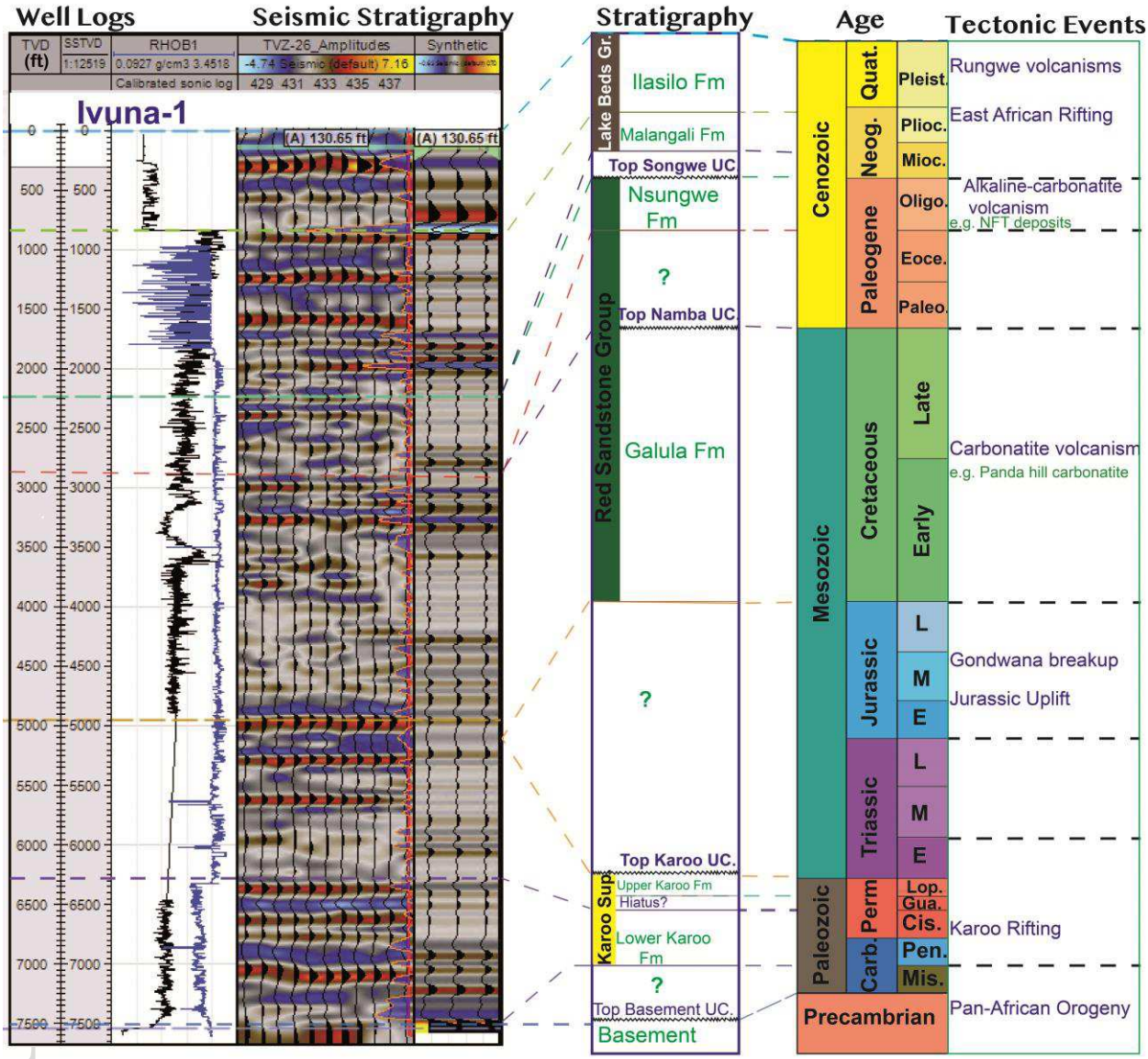

Fig. 2

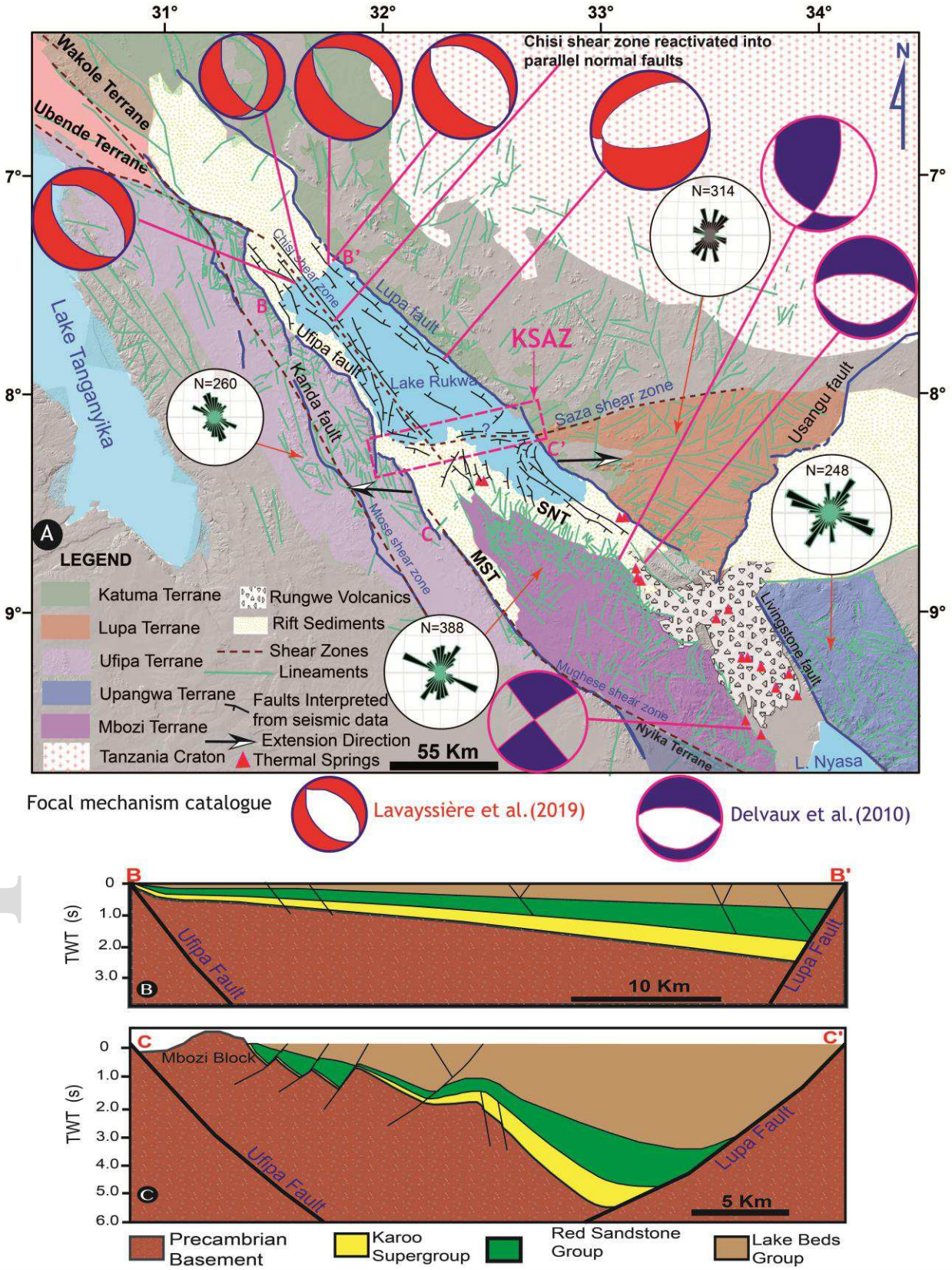

Fig. 3

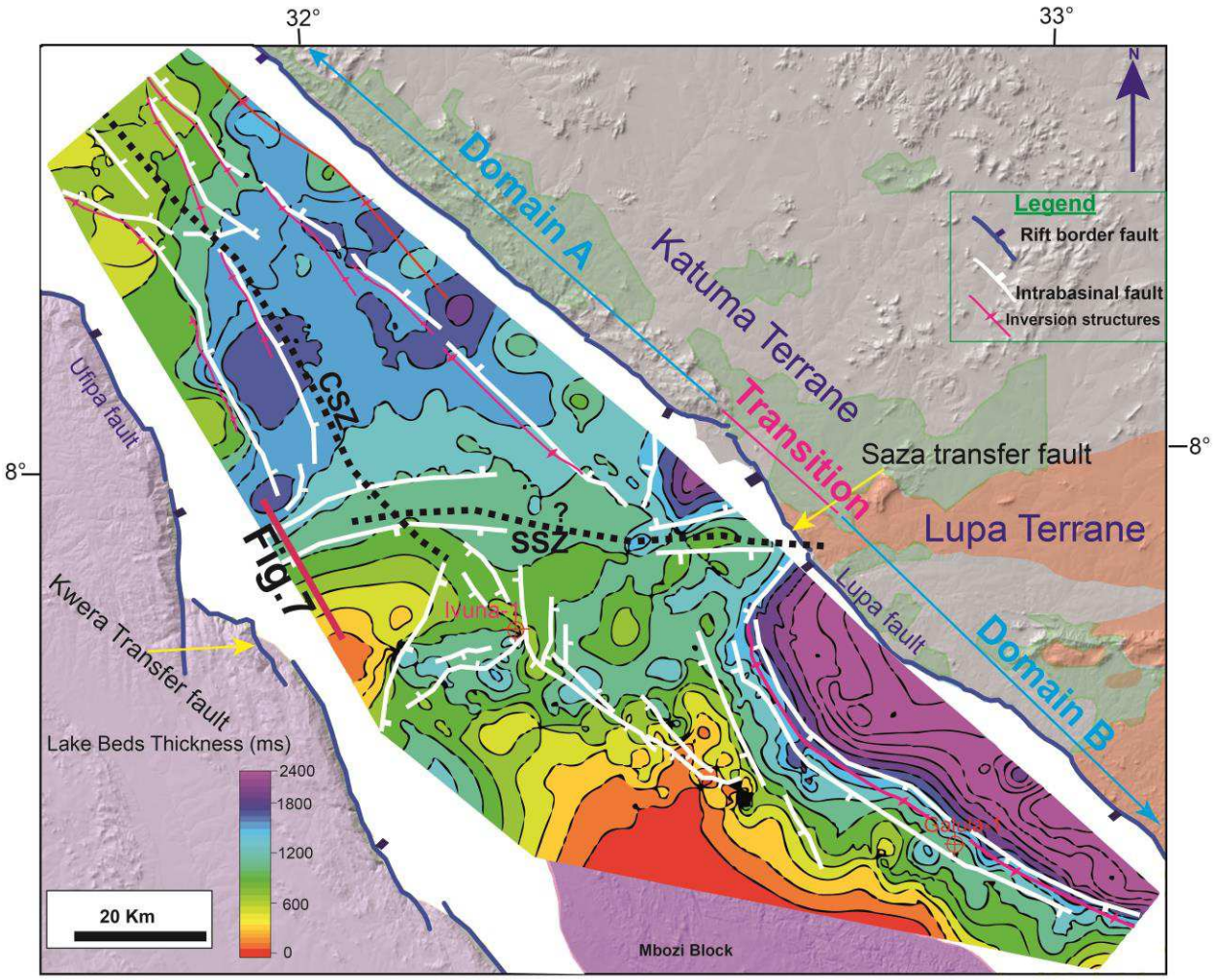

Fig. 4

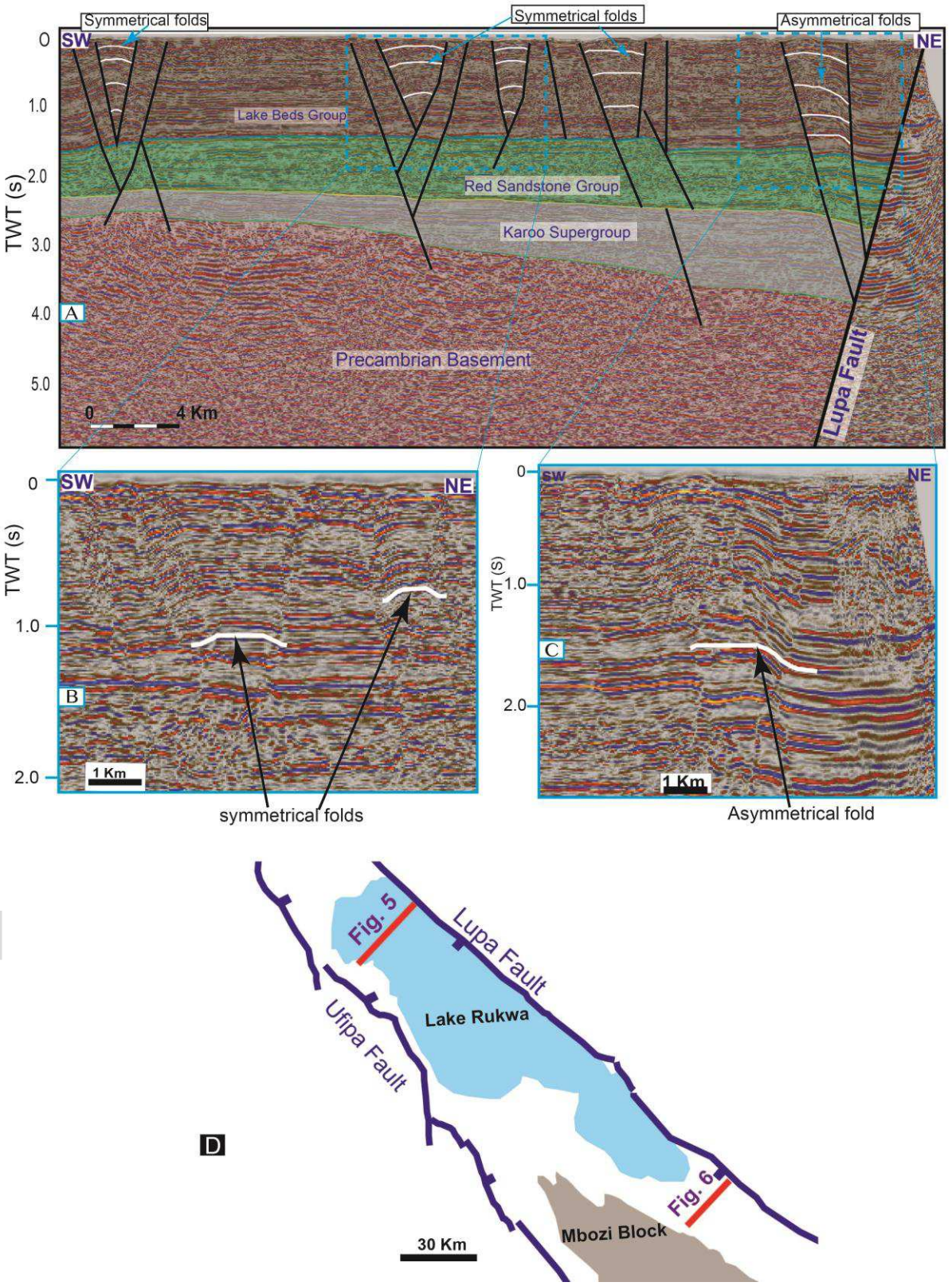

Fig. 5

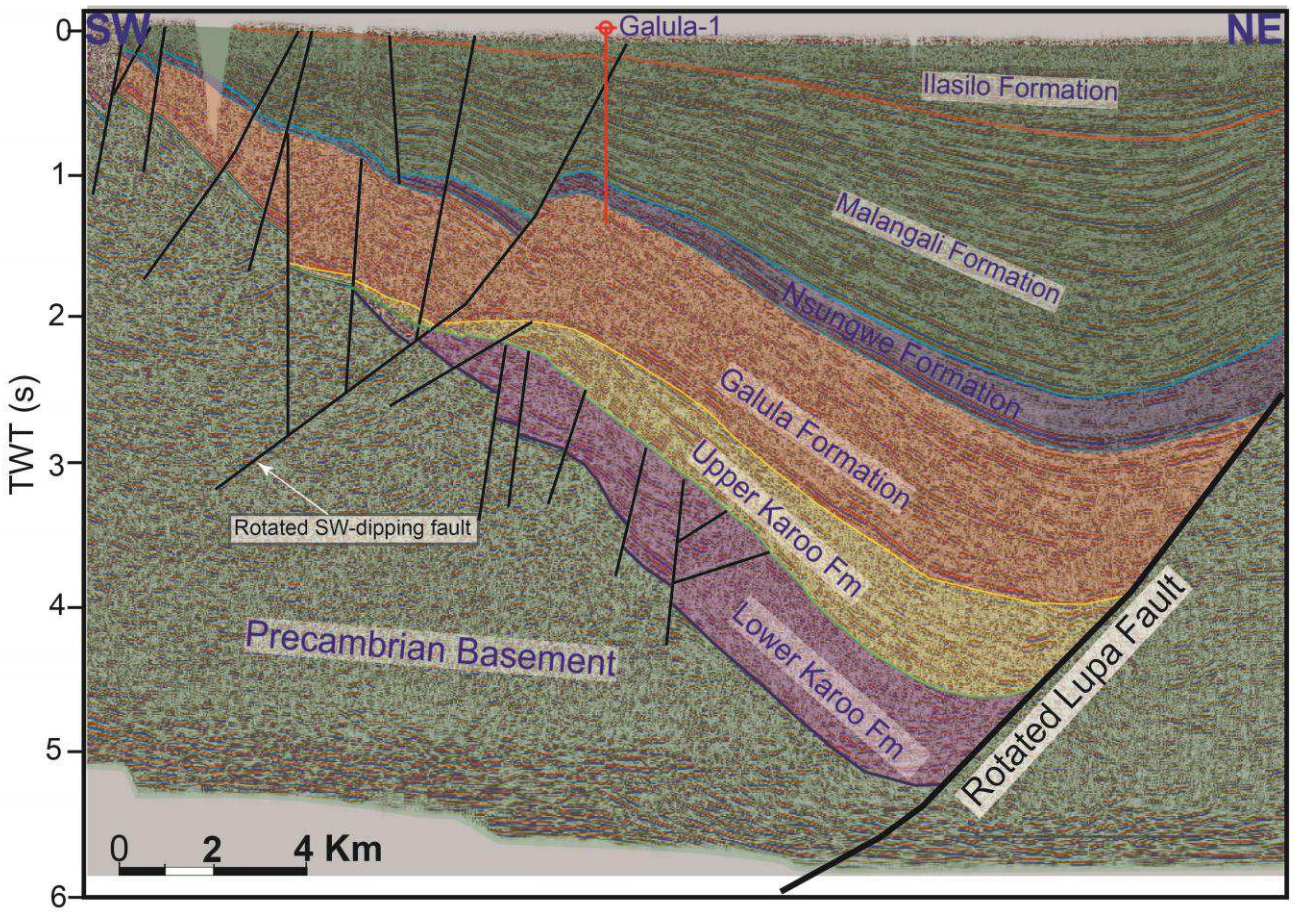

Fig. 6

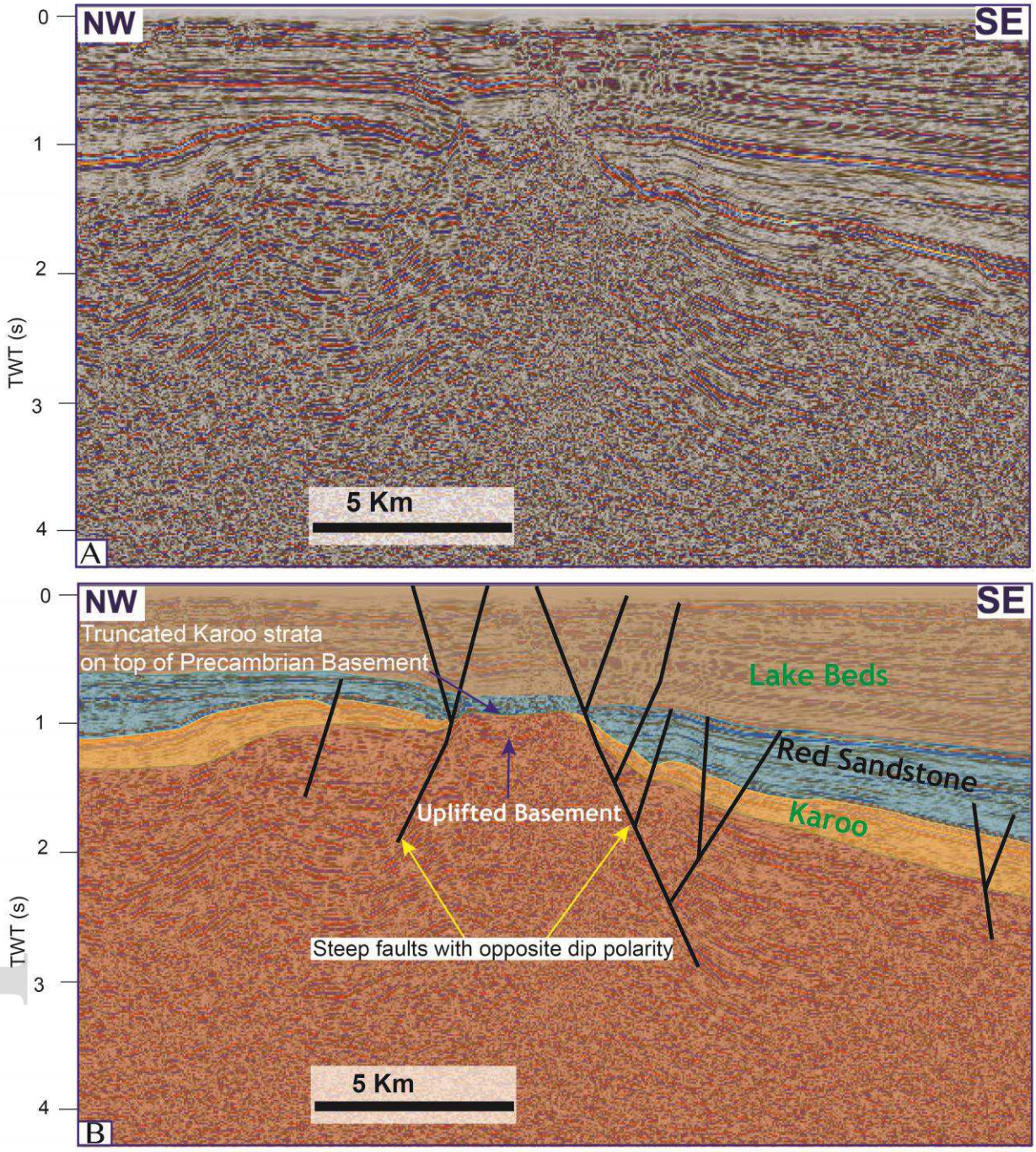

Fig. 7

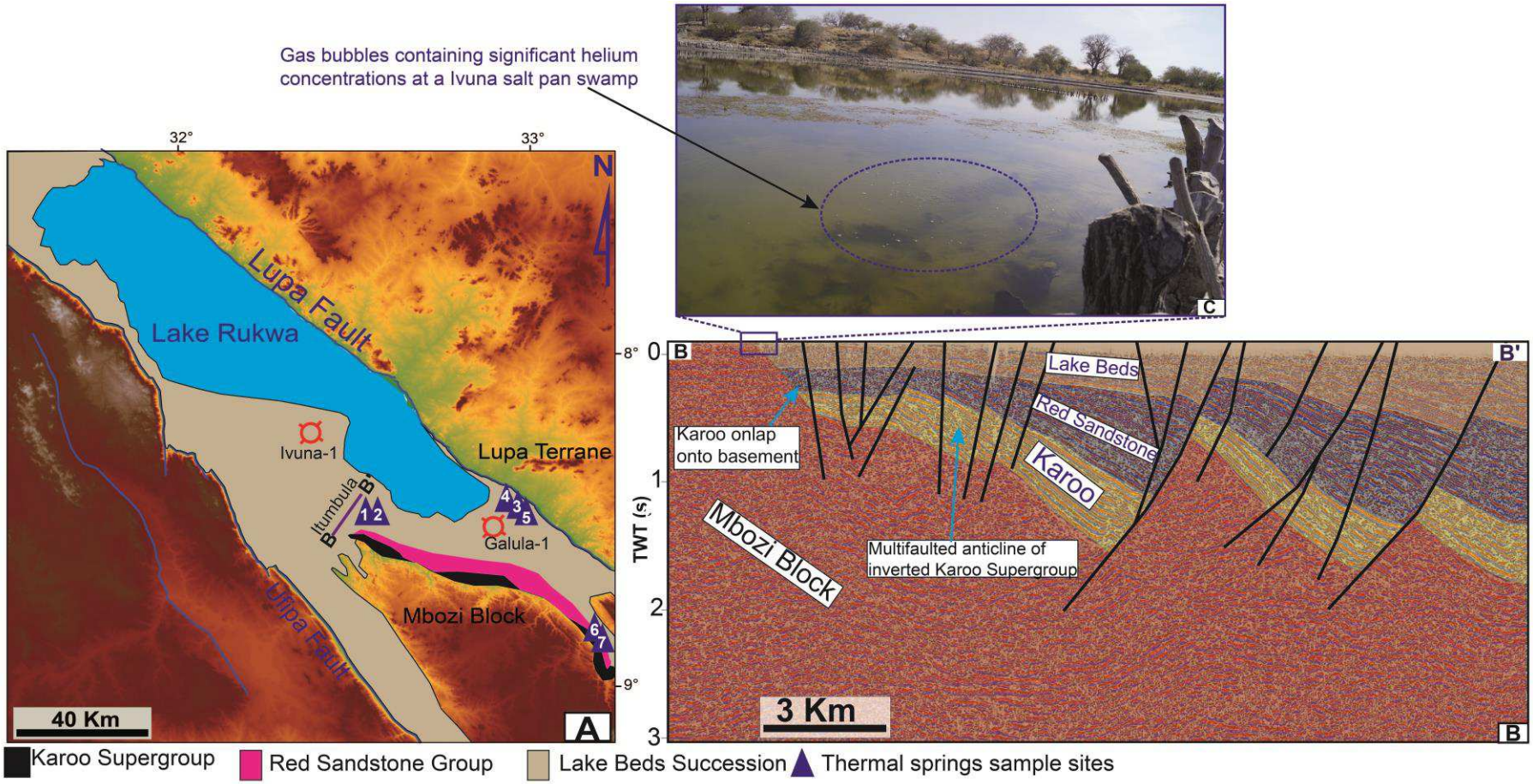

Fig. 8

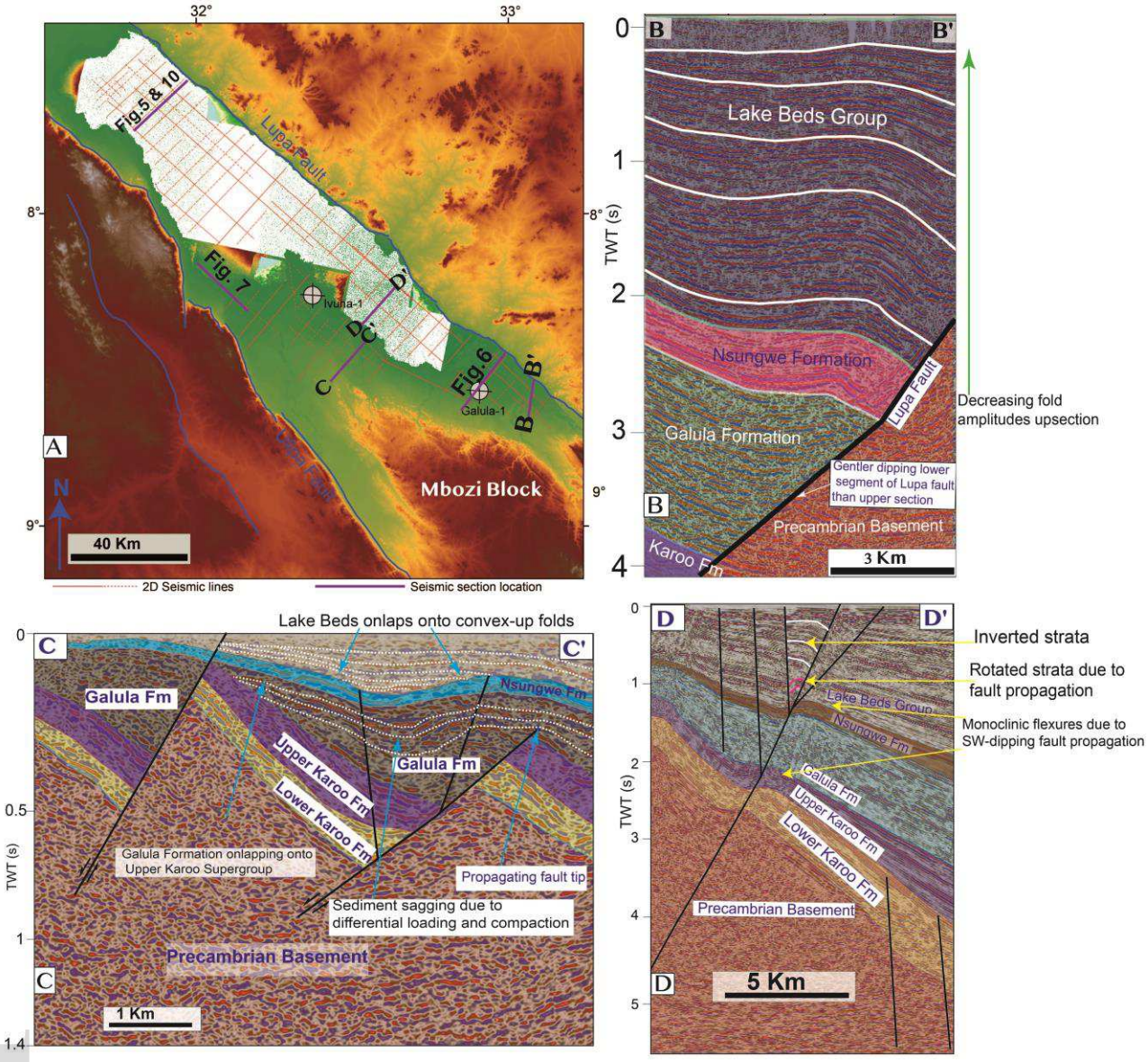

Fig. 9

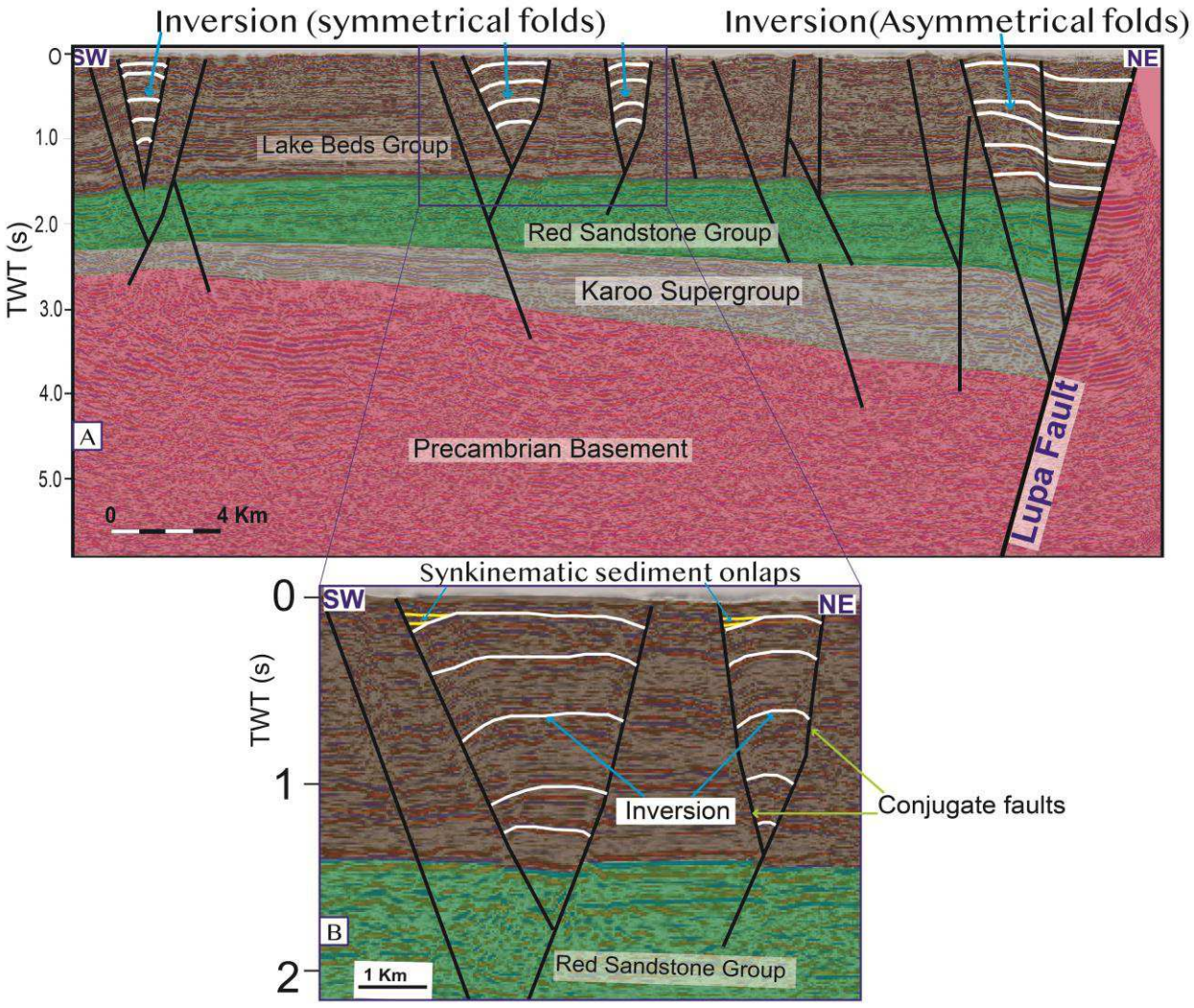

Fig. 10

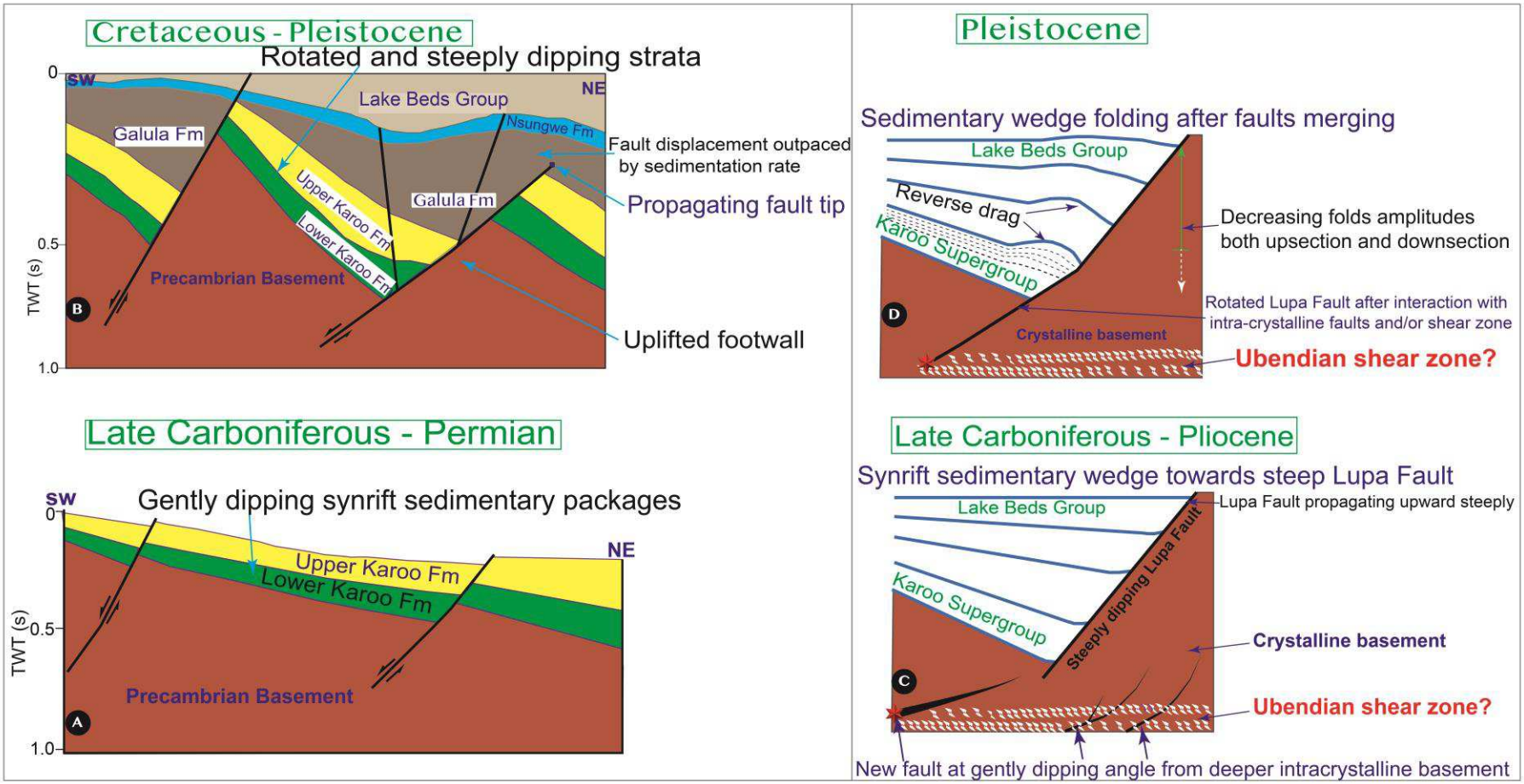

Fig. 11

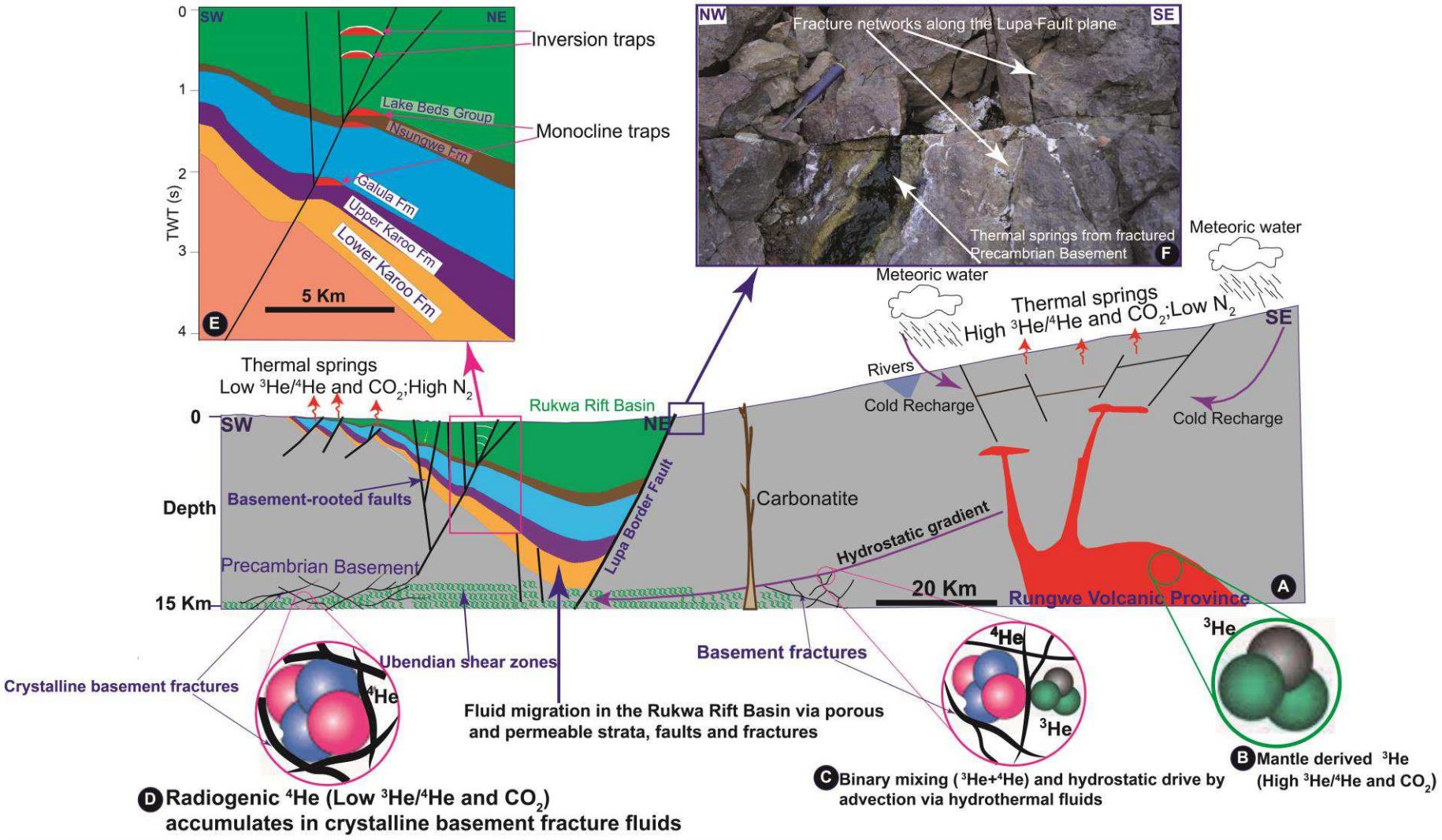

Fig. 12